5.1 Introduction

Gels comprise molecular designs that are proficient at forming 3D spatial arrangement via various chemical interactions; some of the traditional to be mentioned gels are organogel, hydrogel, and supramolecular gels [Hirst *et al.* (2008), Lan *et al.* (2015), Sugiyasu *et al.* (2004), Miyata *et al.* (1999), Sangeetha & Maitra (2005)]. Wherein, metallogel gaining a swift as an imperative bough of supramolecular gels [Tam *et al.* (2013)]. With the distinct choice of gelator moiety and transition metals, they were formed when a metal complex self-assembles by capitalizing non-covalent interactions to fabricate vastly cross-linked, entwined, the three-dimensional framework to immobilize a large number of solvent molecules [Svobodová *et al.* (2012), Venkataraman *et al.* (2011)]. It is valuable to cite that in a sprint towards gel formation, self-assembly progression in a one-dimensional manner engenders fibrous morphology. Introducing functional groups like urea, amide, and aromatic rings, which are capable of shaping various weak interactions like hydrogen bonding or π–π stacking in amid combination of suitable gelator and transition metals, are very much influential in immobilizing solvent.

Meanwhile, multiple coordinating sites in ligands uphold the obligatory cross-linked network in gel, but superficially exo-diatopic ligand with a "one dimensional'' approach in the majority was put into operation for metallogels synthesis [Liu *et al.* (2016)]. This observation goes in opposition to the fundamental principle of gel formation but favors solid polymeric coordination polymers or MOFs, notwithstanding widespread efforts of the hard-working scientific commune.[Kurth & Higuchi (2006)] It is still nearly impossible to predict the design of a gelator molecule like a fixed thumb rule. The Modular character of

metallogel, owe them an assortment of responsive assets with critical potential applications, including chemodosimetry, cosmetics, light-harvesting material, catalytic screening, biochemical and biomedical as well as photonic applications [Whittell *et al.* (2011), Borré *et al.* (2016), Yan *et al.* (2012), Pandey *et al.* (2017), Tam & Yam (2013), Miao *et al.* (2013), Tu *et al.* (2011), Martínez-Calvo *et al.* (2015),Chen *et al.* (2015), Sutar & Maji (2016), Howlader & Mukherjee (2016), Gasnier *et al.* (2009), Steed (2010)].

In contrast, to remarkable physic-ochemical properties such as magnetic, spectroscopic, and catalytic properties, this human-made molecular congregation of soft materials in the utmost of the cases, cannot be directly applied to other useful applications, particularly in electronic devices [Amacher *et al.* (2015), Mitsumoto *et al.* (2017)]. Therefore, the dominance of inorganic materials has stayed ascertained for the fabrication of durable electronic devices [Sun *et al.* (2017)]. Nonetheless, in a pursuit to augment performance and miniaturization of the device and to reinstate the usual inorganic semiconductors, technological advancement attains newer heights towards organic/plastic electronics with functional materials of natural origin. A very few reports were taken up on gel-based π-systems with high conducting properties in oligo(thienylenevinylene) based-organogelator by Ajayaghosh and his co-workers [Praveen *et al.* (2016), Siddhanta & Gangopadhyay (2005)]. In a very similar manner, nanorods and nanotapes with soaring charge carrier mobility were observed as well, while Zang and co-workers performed the groundbreaking synthesis of perylenebisimide-based photo conducting nanofibril, nanoribbons and nanobelts [Che *et al.* (2007)]. An apparent severity in sophisticated molecular designing and synthesis, with tedious optimization to avoid charge carrier

recombination of the intermolecular assembly, makes them very much unreasonable towards large-scale application. [Beaujuge & Fréchet (2011)]

Performances of semiconducting materials are crucially dependent on movement efficiency of charge carriers poignant within the assembled π-conjugated system and hence developing effortless schemes towards the fabrication of photo-conducting materials [Mitsui *et al.* (2014)]. In this article, we reveal the preparation of a Schiff base derived polymeric coordination gel, with high efficiency *en-route* to functioning as semiconducting devices. Reports on conducting gels are escalating but homologically constrained to systems like tetrathiafulvalene (TTF), thienylenevinyle, etc. Here we have been able to apply these materials successfully in metal-semiconductor junction thin-film devices to study the electronic device applicability and charge transport properties of the synthesized material. The current-voltage characteristics of our fabricated devices depict a non-linear rectifying nature, similar to a Schottky barrier diode with a sound rectification ratio [Bhattacharya *et al.* (2014), Dhibar *et al.* (2018)]. Hence we have analyzed the device performance of our fabricated Co metallogel based Schottky diode.

5.2 Instrumentation

Electronic absorption spectra was obtained on a Thermo scientific EVOLUTION 201 spectrophotometer. ^{1}H NMR spectra was collected on a Bruker AVANCE III HD 500 spectrometer. Electrospray ionization mass (ESI-MS) spectra were recorded on a Waters (Micromass MS Technologies) QTof Premier. Thermal Gravimetric analysis data was acquired on a NETZSCH STA 449 F3 at a heating rate of 5 °C min^{-1} under a nitrogen atmosphere. TEM images. Powder XRD data were collected on Rigaku MiniFlex 600

Detector D-tex ultra between angle 2θ = 5-80°. Solution electrical conductivity was measured on a Eutech Instruments CON 5/TDS 5 Conductivity Meter. The instrument was calibrated with standard solution. All rheological measurements of metallogel were performed on Anton Paar MCR 702 Twin Drive Rheometer. A Kiethley Source meter model number 2612 was used to perform the current-voltage (I–V) characteristics of our manufactured coordination polymeric gel material based thin film devices.

5.3 Experimental Section

5.3.1 Method

5.3.1.1 Synthesis of Gelator SHAL

To a methanolic suspension of adipoyl hydrazone (1.00g, 6.8 mmol), 2 mL water is added to obtain a clear solution. 2-hydroxybenzaldehyde (1.67 g, 13.6 mmol) was added to this solution and refluxed for 1 hour. The precipitate obtained after cooling to room temperature was filtered, thoroughly washed with Chloroform, methanol, and Hexane to afford a white solid (AL), Yield 1.74 g (81 %). Due to deprived solubility of the neutral form, UV-vis measurements is performed by dissolving the solid in DMF in the presence of 1 Equivalent of LiOH [Pandey *et al.* (2019)].

5.3.2 Synthetic Scheme of Gelator

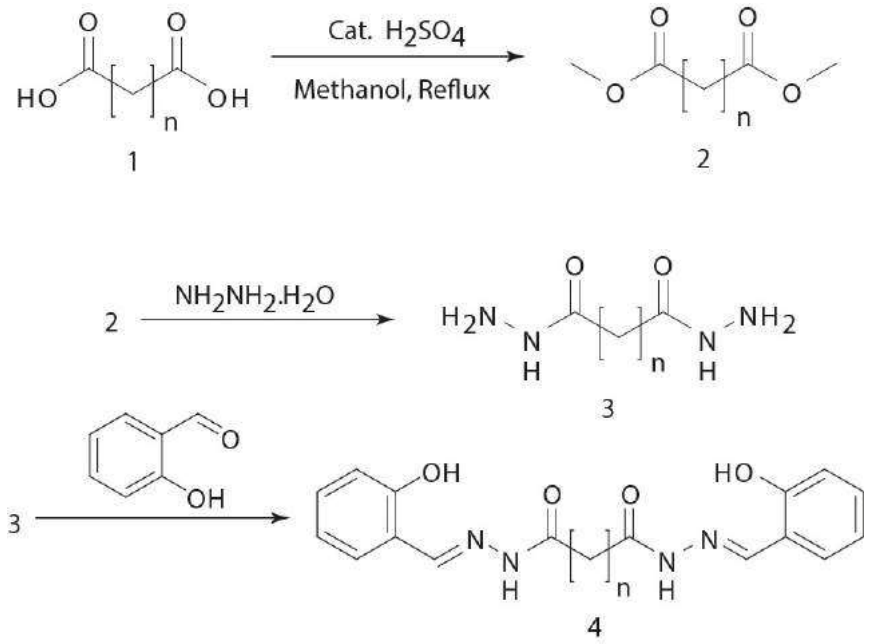

Scheme 5.1 Synthetic Strategy adopted for the synthesis of gelator SHAL

5.3.3 Preparation of metallogel

An unambiguous, transparent solution was prepared upon mixing SHAL (10 mg, 0.026 mmol) in 0.5 mL DMF and 4 equivalents LiOH (4.37 mg, 0.10 mmol in 0.25 mL DMF) followed by brief sonication. For gelation, a solution of $Co(OAc)_2 \cdot 4H_2O$ (6.94 mg, 0.026 mmol in 0.25 mL) was added instantly to previously prepared mixture of SHAL deprotonated with LiOH, a translucent & non-fluorescent brown color gel (1% w/w) was formed within a minute at room temperature under atmospheric pressure (Figure 5.1). The CoA-SHAL coordination polymeric gel was stable for an extended period of even two weeks.

5.4 Results and Discussion

5.4.1 Characterization

The synthesized metallogel is characterized by various instrumental techniques such as ^{1}H NMR and IR spectrometry **(**Figure 5.2**)**.

5.4.2 ^{1}H-NMR and IR spectrum of gelator

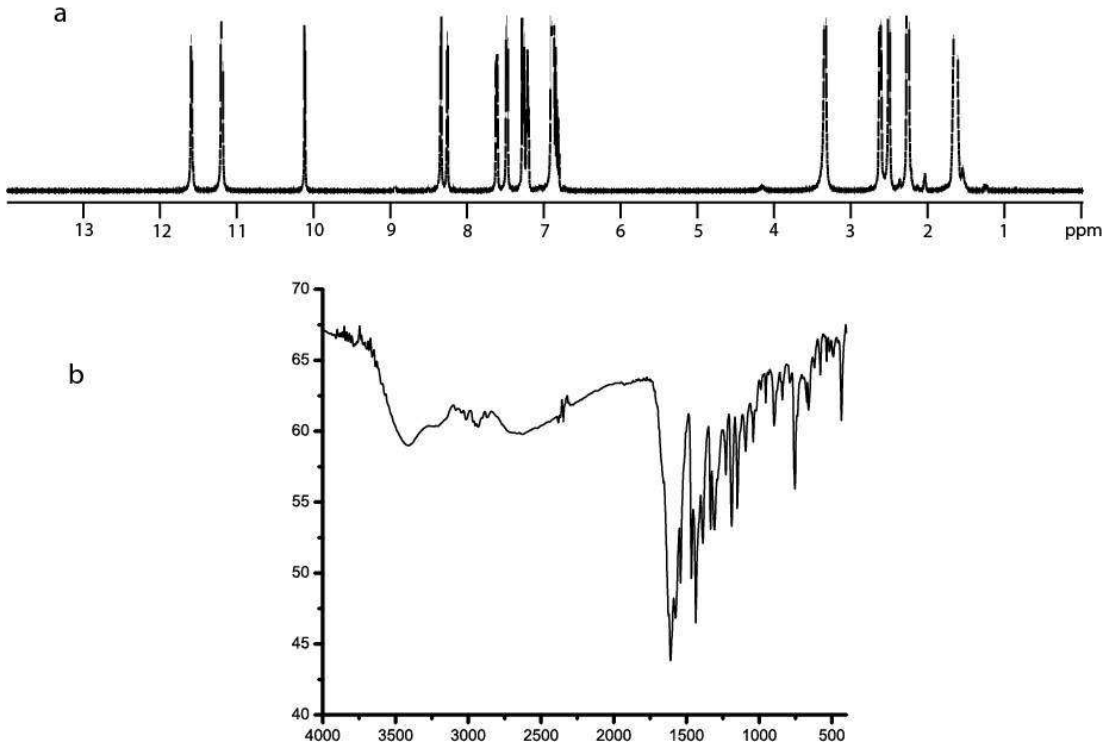

Figure 5.1 ^{1}H NMR and FTIR spectra of gelator SHAL

5.4.3 Comparative IR of gelator and metallogel

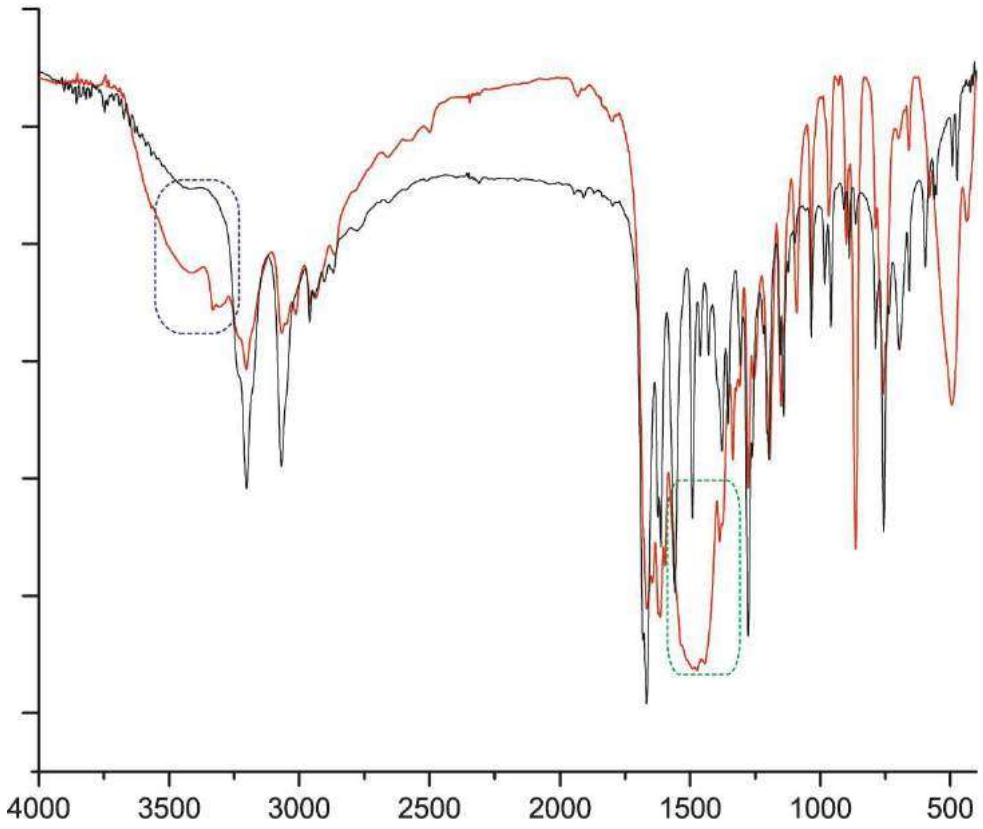

Figure 5.2 Comparative IR spectra of gelator (black) and xerogel (red) showing coordination of Co^{2+} through O, N, O binding core

FTIR spectral analysis (Figure 5.3) of Schiff base gelator (SHAL) shows characteristic bands of υ(–OH), υ(–NH) at 3407 cm^{-1} and 3206 cm^{-1}, respectively, while active band at 1669 cm^{-1} is corroborated to υ(-C=O) group, in addition to peaks as mentioned earlier υ(–C=N) is observed at 1553 cm^{-1} which suggest the enolic form of ligand. A comparative study of FTIR spectra of gelator and xerogel SHAL indicates the disappearance of –OH band, broadening of aforementioned N-H band, and shifting of υ(–C=O) to 1606 cm^{-1} ($\Delta\upsilon$ = 53 cm^{-1}) which may be attributed to the coordination of Co^{2+} through O, N, O binding

core. Alkali base (4 equiv.) is required for deprotonation signifies the tetra basic hexadentate nature of ligand as it is a necessary condition for coordination of a metal ion through deprotonation of both phenolic and -NH labile protons adjacent to azo-methine group [Pandey *et al.* (2019)].

5.4.4 Mechanical Properties of metallogel

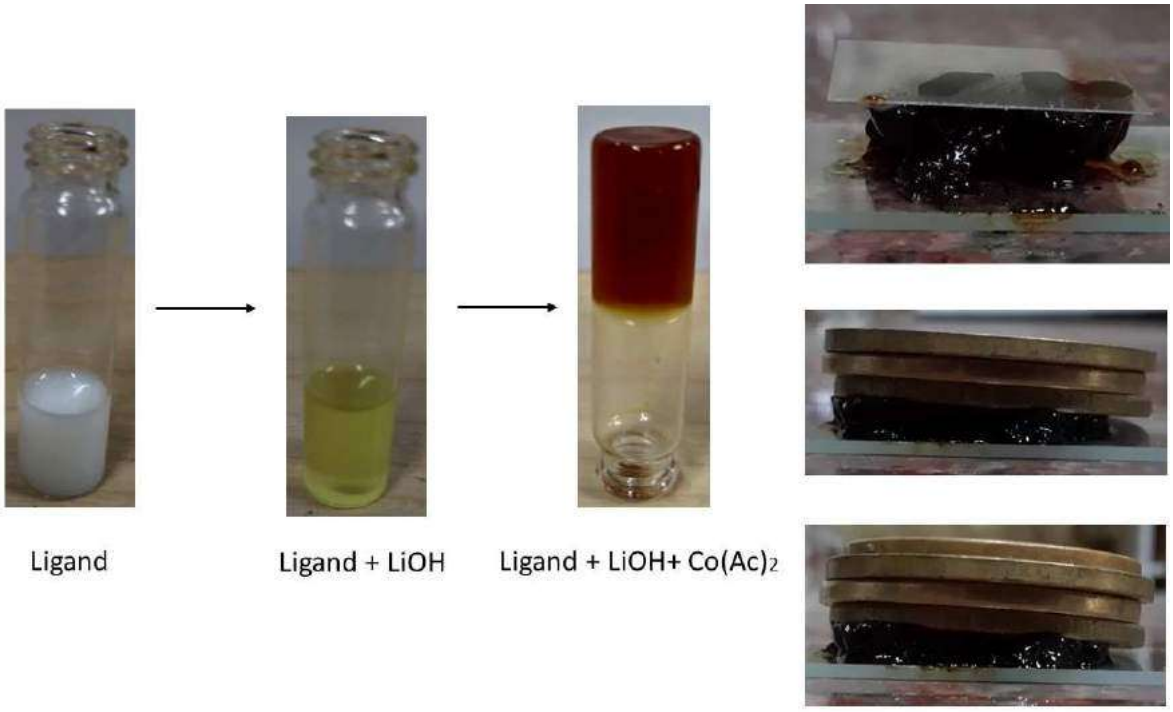

Figure 5.3 mechanical and load bearing properties of Cobalt containing metallogel

Excellent load-bearing and mechano-responsive behavior is observed with metallogel. Gel formation was extremely fast without the help of any external stimuli.

5.4.5 Morphology of Metallogel

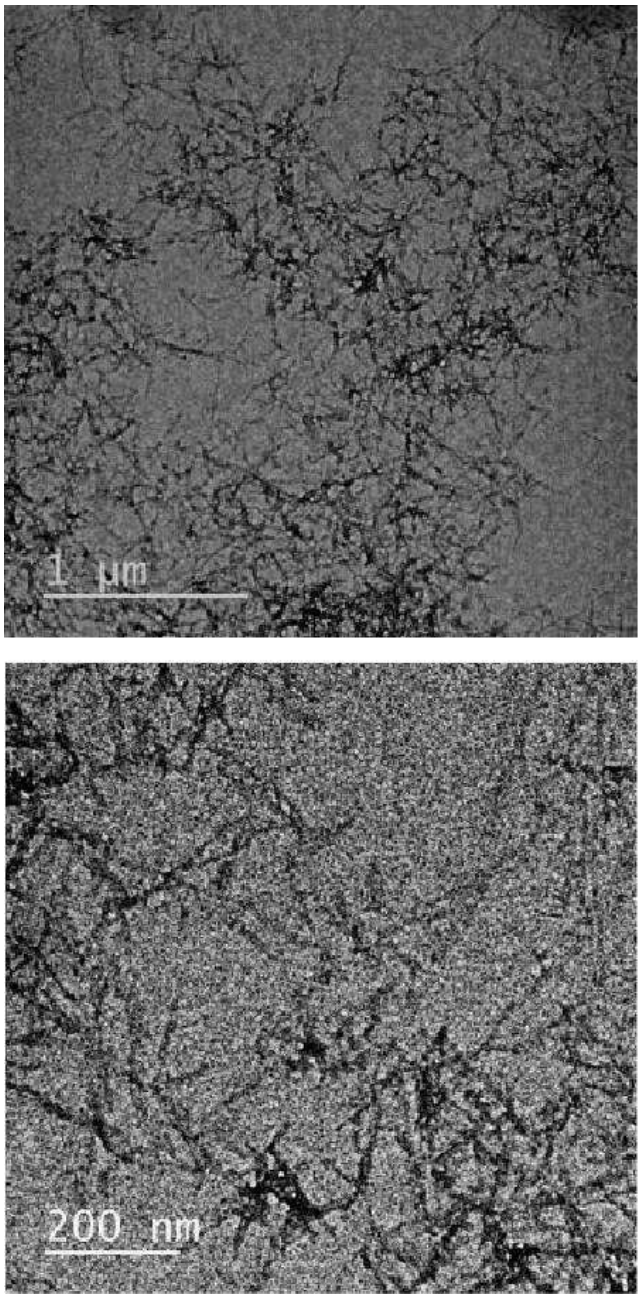

Figure 5.4 TEM pictures of diluted metallogel (SHAL/LiOH/$Co(OAc)_2$; ~10^{-3} M) under three different magnifications

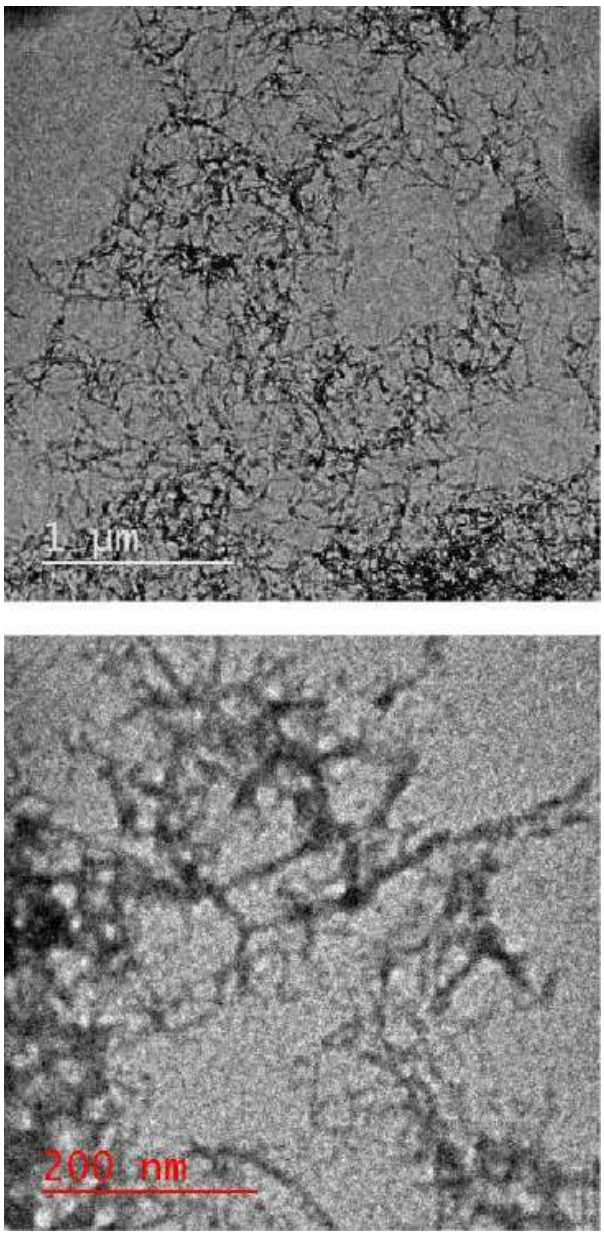

Figure 5.5 TEM pictures of diluted metallogel (SHAL/LiOH/$Co(OAc)_2$; ~10^{-3} M) under three different magnifications

Unambiguous morphological insights of obtained metallogel is examined under Scanning Electron Microscopy (SEM) and transmission electron microscopy (TEM). Interesting observations are obtained upon its comparison to our previously reported work.

Morphology revealed by SHAL derived gel was also in line with the above statement, where TEM (Figure 5.5) revealed the bunch of extended and interconnected fibers with close-knitted appearance. TEM (Figure 5.6) study on diluted metallogel revealed the three-dimensional (3-D) network of nanofibers of about ~25 nm in average diameter with an intermingled appearance

5.4.6 UV-vis Spectroscopy

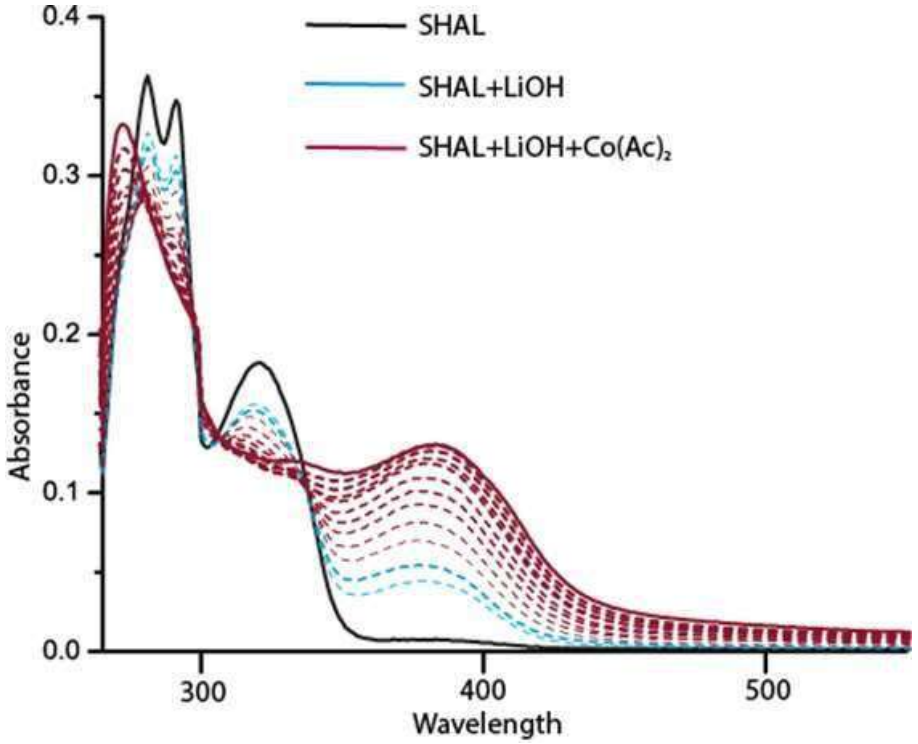

Figure 5.6 UV-vis titrations in DMF (a) ligand SHAL, (black line; λ_{max} 320 nm; $1x10^{-5}$ M), deprotonation with LiOH (4 equiv., blue line) and upon aliquot addition of $Co(OAc)_2$ (red line) band corresponding to ligand diminishes ratio-metrically with appearance of new peak at 388 nm along with fine isosbestic point

To prove the complexation between SHAL and Co(II) as well as gelation behavior, we executed detailed electronic absorption studies. Exposition of two vividly coupled bands by SHAL ($1x10^{-5}$ M, DMF, 298 K) at λ_{max}=280 nm and 291 nm are accredited to intraligand

π-π* transition while a less intense band at 320 nm endorsed n-π* transition [Pandey *et al.* (2017)].

Alternatively, splitting of the peak at 280 and 291 nm elucidate dissimilar planarity of both hydrazones, i.e., both free hydrazones exist in anti-cis configuration. Inconsequential variation in spectra are observed upon deprotonation of SHAL ($1x10^{-5}$ M, DMF) with 4 eq. LiOH, i.e., a light yellow colored solution of SHAL displayed a hump at about 394 nm with a concomitant decrease of the 320 nm band along with the ratiometric increase of hump. It indicates deprotonation of phenolic –OH as well as chelation of Li^{+} with SHAL in N,O fashion. While upon aliquot addition of $Co(Ac)_2.4H_2O$ ($1x10^{-3}$ M, DMF) to this solution, the disappearance of band at 320 nm is observed with ratiometric emergence of a new peak at 388 nm ($\Delta\lambda$ = 68 nm) (Figure 5.7). Two nice isosbestic points at 305 and 344 nm indicate the presence of equilibrium between two species during their transformation to the coordination complex. The endpoint of UV titrations is found to be 1.0-1.2 equivalent indicated the formation of a coordination complex, between Co(II) with SHAL at 1:1 ratio. Stoichiometry model for Co^{2+} complexation with gelator SHAL demonstrated through Job's plot was found in good agreement to above spectroscopic result where the gelling combination was found close to 1:1 metal to ligand ratio (Figure 5.8**)**.

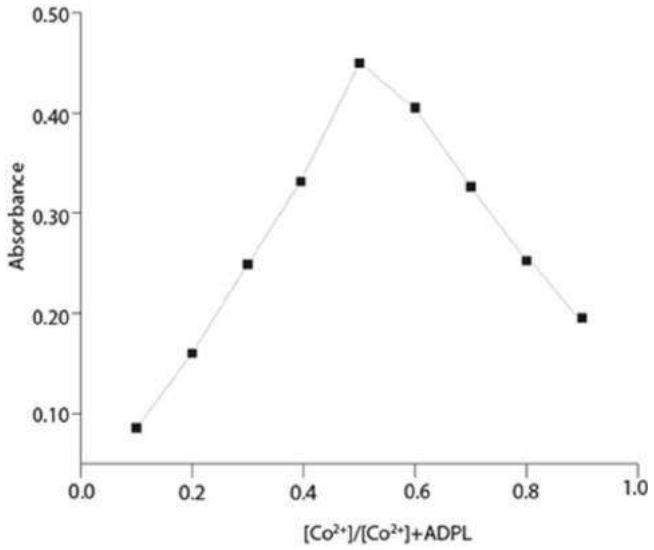

Figure 5.7 Job's plot diagram of [Co^{II}]/[Co^{II}]+[SHAL]

5.4.7 Emission Spectroscopy

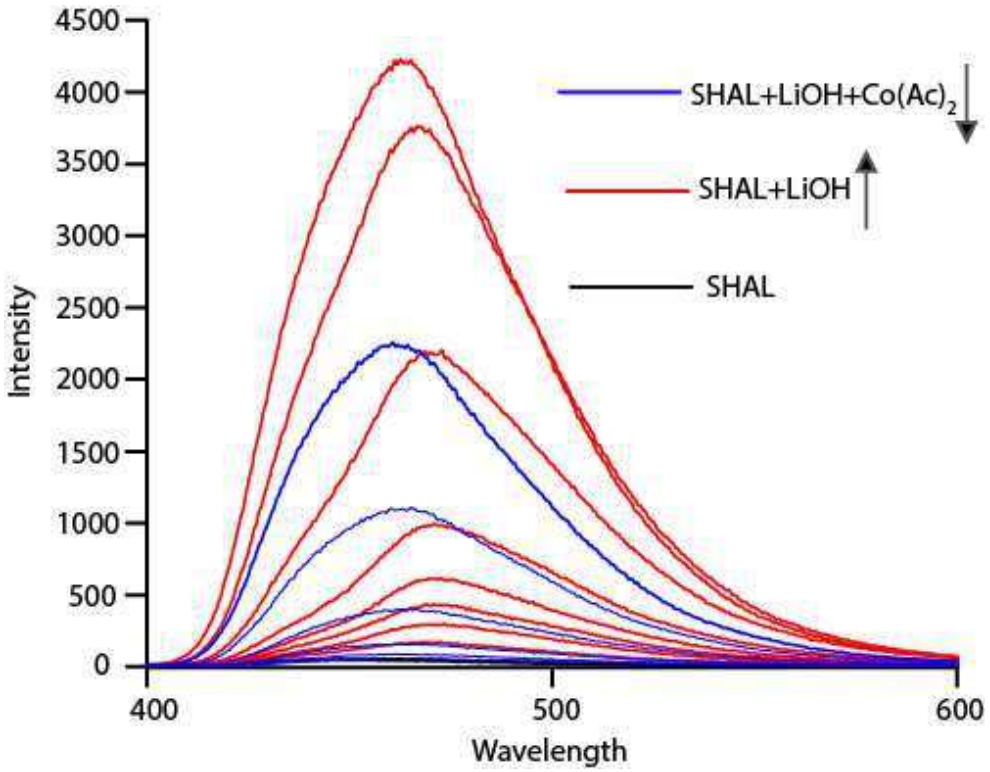

Figure 5.8 Fluorescence spectra in DMF (Red line = deprotonated ligand, Blue line = Metal addition (λ_{ex} = 320 nm)

In the course to reconnoiter the aggregation behavior as well as mechanistic acuity towards gelation, fluorescence experiment were performed over non-fluorescent metallogel (Figure 5.9**)**. The non-fluorescent nature of SHAL (λ_{ex}=320 nm, λ_{em}=477 nm, stokes shift= 10300 cm^{-1}; $1x10^{-3}$ M, DMF, black line) transformed subsequently to bluish-green fluorescent solution upon ratio-metric deprotonation with LiOH (10^{-1} M, DMF, red line) and showed peak at 471 nm (stokes shift= 10150 cm^{-1}; red line) with noticeable enhancement in fluorescence intensity which can be credited to chelation of Li^{+} to AL^{2-} and can be ascribed to well-known phenomenon of chelation enhanced fluorescence (CHEF) as in our previous report where large enhancement of fluorescence is observed through CHEF upon LiOH addition to the ligand. Further, we observed quenching upon addition of the requisite amount of Co^{2+} (10^{-1} M, DMF, blue line) required for metallogel formation (λ_{em}=468 nm, stokes shift= 9900 cm^{-1}; blue line) indicates the presence of ACQ phenomenon in gelation process [Pandey *et al.* (2017)].

5.4.8 ESI Mass analysis of metallogel

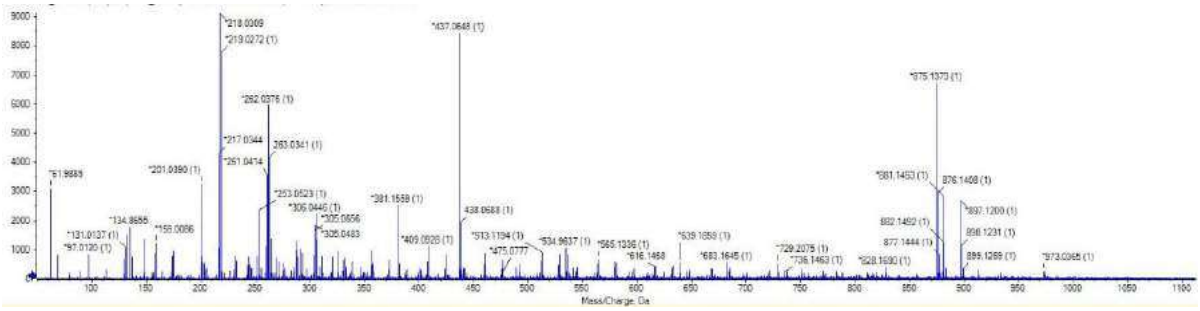

Figure 5.9 ESI-MS spectra of $[(C_{20}H_{21}N_4O_4)Co_2Li_5)]^-$ at 534.96 represents the experimental isotopic abundance pattern 1:1 polymeric coordination SHAL vs Co^{2+} repetitively (1 ligand + 2 metal ion in one asymmetric unit)

To ensure the formation of coordination complex indicated by UV-vis and Job's plot, we performed detailed ESIMS spectral analysis over diluted metallogel. ESI-MS spectra of

$[(C_{20}H_{21}N_4O_4)Co_2Li_5)]^-$ at 534.96 represents the experimental isotopic abundance pattern 1:1 coordination polymeric SHAL vs. Co^{2+} in a repetitive manner.

5.4.9 Rheology

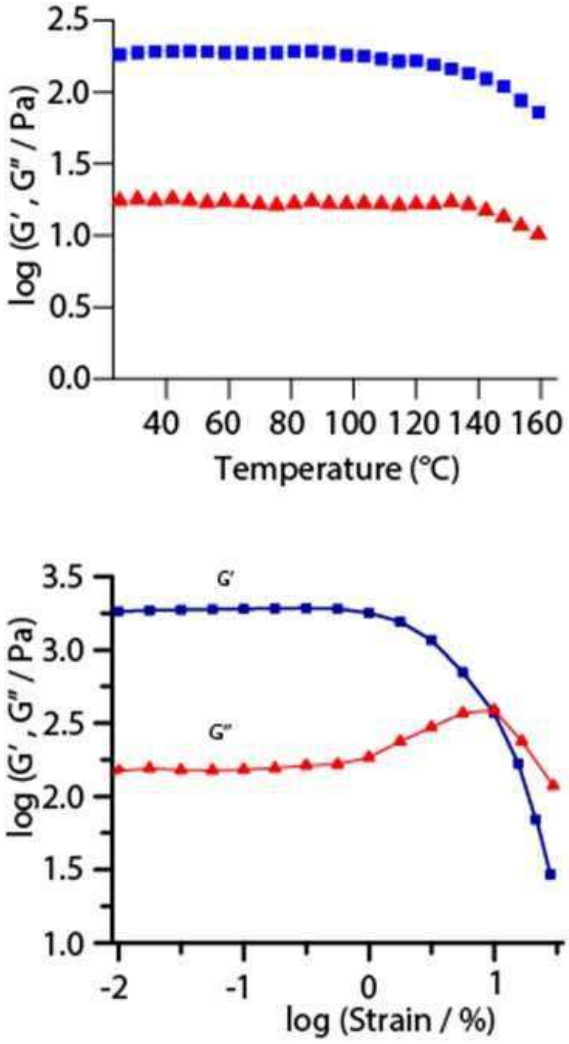

Figure 5.10 (upper) Dynamic temperature ramp G' and G'' for SHAL-Co gel at heating rate of 1°C min^{-1}, strain of 0.5% and frequency of 1 rad s^{-1}, (lower) Dynamic oscillation strain sweep of G' and G'' for gel at frequency of 1 rad s^{-1} and 25 ° C

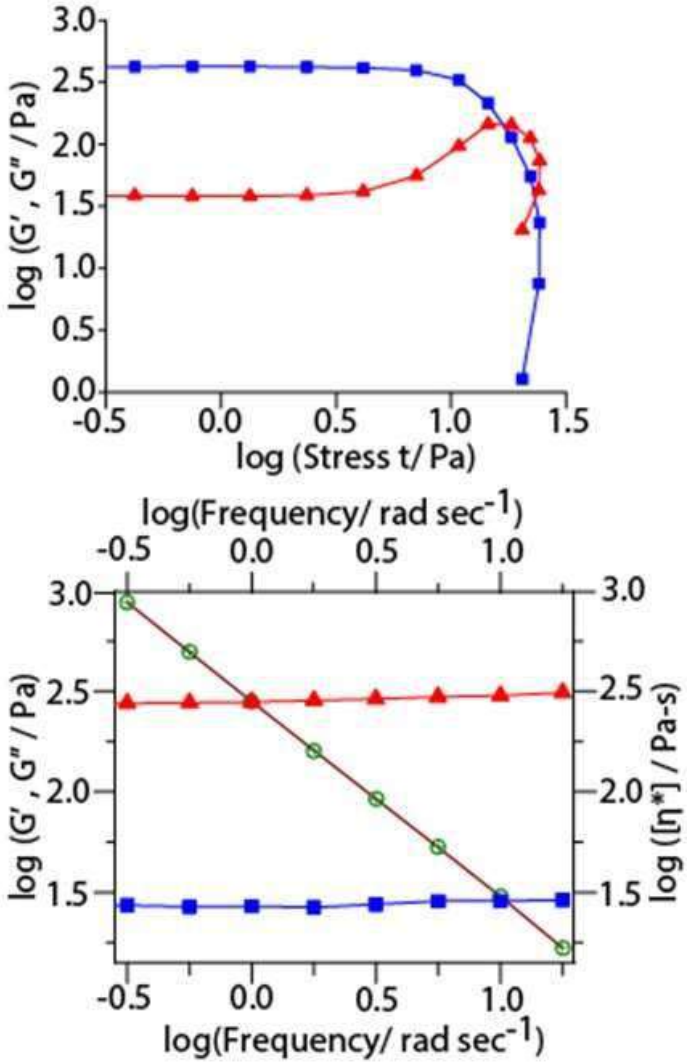

Figure 5.11 (upper) Dynamic shear stress of G' and G'' for gel, (lower) Dynamic frequency sweep measurement of G' and G'' for SHAL-Co gel at strain of 0.5%. Secondary axis: complex viscosity measurements

Rheological experiments are conducted over freshly prepared (1.0% w/v) fixed concentration metallogel. Implementation of frequency sweep measurements between 0.1 and 100 rad s^{-1} at 25°C within the linear viscoelastic region indicated that G' and G'' values were linear and increase slightly within the applied frequency (f) range (-1.0-2.0 rad s^{-1}) principally supporting its elastic nature. Furthermore, G' is dominating G'' and they do not

cross each other, suggesting any phase separation or transition, which is anticipated for a stable and rigid gel phase material. Further evidence of elasticity was visualized by the fact that G' and G'' are very less sensitive to angular frequency (ω). Variation tendency of both storage modulus (G') and loss modulus (G'') with increasing temperature was recorded from temperature range 25-160°C. As shown in (Figure 5.11), both values remain unaffected up to 120° C and above which both G' and G'' decreases with an inclination in temperature, indicating liquefaction. Storage Modulus (G') and loss modulus (G") are obtained at 25°C and 1 rad s^{-1} as a function of shear stress and strain (Figure 5.11 and 5.12). Metallogels when subjected to oscillatory shear, value of G' was found be higher than G'' by order of ~1 magnitude of shear stress. It is in accordance with the exact gel phase where no variation among G' and G'' was observed with appreciable long range of increasing applied stress. At yield stress of ~1.3 Pa G' and G'' intersect each other establishing a mechanical breakup of gel beyond which the deviation from linearity results in a gel-sol phase transition. On the other hand, both in-phase storage modulus (G') and out-of-phase loss modulus (G'') remain constant up to 0.9% (G'>G''), beyond which deformation of network occurred.

5.4.10. Optical characterization

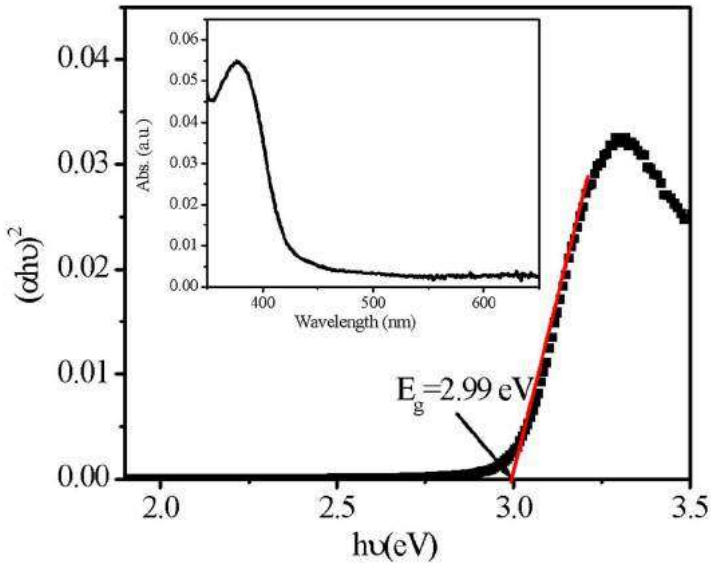

Figure 5.12 Electronic absorption spectra (inset) and Tauc's plots for semiconducting gel film

To examine the spectral property and estimation of the bandgap, the electronic absorption spectrum of thin film was recorded in the range 250–600 nm using UV-vis spectrophotometer [Radecka *et al.* (2008)] as shown in Figure 5.13, The direct optical band gap of the film can be calculated by applying Tauc's equation,

$$(\alpha h\nu)^2 = A\,(h\nu - E_g)$$

where α, E_g, h and ν denotes absorption coefficient, the band gap of materials, Planck's constant, and frequency of light, respectively. We have extrapolated the linear region of the plot $(\alpha h\nu)^2$ vs. hν, as demonstrated in Figure 5.13. The value of E_g of the film of the material has been calculated as 2.99 eV.

5.4.11. Electrical Characterization

Our previous investigation in this report and published literature suggests that our synthesized complex is an n-type semiconductor material in nature. Therefore, we have fabricated the sandwiched structure of the metal-semiconductor junction using suitable electrode materials and studied its electrical properties by analyzing the charge transport behavior [Kahn *et al.* (2003)]. It is worth here to mention that the junction properties of semiconducting materials were determined by the interfacial properties of two electrodes used for device fabrications and the difference of their respective work functions [Tada et al. (2011)]. Therefore, for fabrications of a diode having rectifying behavior, one should select an electrodes materials in such a way that one electrode work as ohmic contact and other electrode creates non-ohmic Schottky contact with semiconducting layer. As per the theory of the Schottky barrier, the work function of the metal electrode should be higher as compared to the n-type semiconductor for the creation of a rectifying barrier at the interface [Tongay *et al.* (2012)]. As stated in published articles, the work function of indium tin oxide (ITO) is comparable with our materials and form an ohmic contact. However, gold (Au) creates rectifying contact due to a higher work function. Therefore, we select these materials for the formation of rectifying Schottky diode [Lu *et al.* (2006)].

The current density-voltage (J-V) measurements of our synthesized complex based multiple devices are recorded at a corresponding applied bias voltage sequentially within the limit ±2 V and analyze for various electrical parameters [Aswal *et al.* (2006)]. The J–V characteristics of the synthesized complex-based devices have been investigated at room temperature under the dark condition and are demonstrated in Figure 5.14 the recorded J–V characteristics of the Au/semiconducting gel interface show an asymmetrical nonlinear

nature curve, which is the validation of a rectifying Schottky barrier diode (SBD). We have calculated the rectification ratio (I_{on}/I_{off}) of our device and found to be 266±15, which is very good for the semiconducting gel-based newly fabricated device [Capozzi *et al.* (2015)].

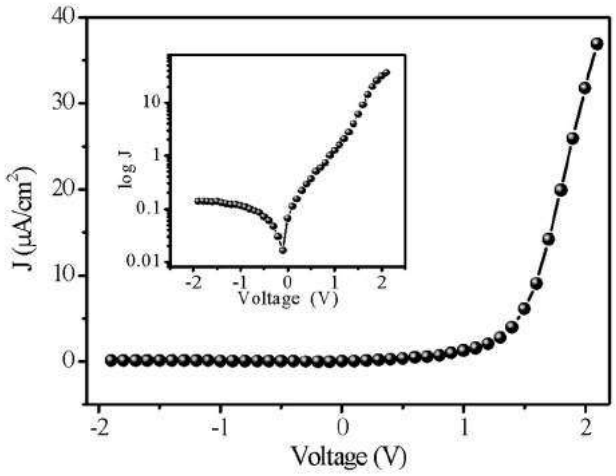

Figure 5.13 J–V characteristics curve for ITO/complex/Au structured thin film devices at room temperature

The obtained rectifying J-V characteristics of semiconducting gel at room temperature were further analyzed by assuming the standard thermionic emission theory and Cheung's method and extracted critical electrical parameters of the device. [Dragoman & Dragoman (2004)] To analyze J-V curves quantitatively, we have first employed the following standard equations:

$$J = J_0 \exp(\frac{qV}{\eta kT})(1 - \exp(\frac{-qV}{\eta kT}))$$

At room temperature, $J_0 << 1$. Therefore

$\eta = \frac{qdV}{kTdln(J/J_0)}$ and

$J_0 = A^*T^2\exp(\frac{-q\Phi_B}{kT})$ or $\Phi_B = \frac{kT}{q}\ln(\frac{A^*T^2}{J_0})$

where J_0, k, T, V, A, η, and A* demonstrate the reverse saturation current, electronic charge, Boltzmann constant, temperature in Kelvin, forward bias voltage, ideality factor, and effective Richardson constant, respectively. The effective Richardson constant may be considered as 32 A K^2 cm^{-2} for the semiconducting gel-based devices.

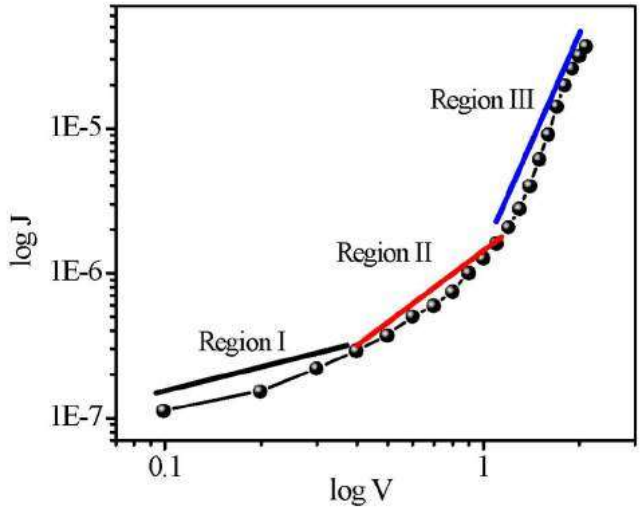

Figure 5.14 Double log plot of J-V characteristics.

Table 5.1 Electronics parameter of device

Device	η	J_0 A/cm^2	Φ_B(eV)	M (cm^2/V.s)	I_{on}/I_{off}
ITO/SG/Au	3.1	$1.64x10^{-8}$	0.89	$4.36x10^{-4}$	266±15

In the forward region, current increases exponentially while in reverse region current do not follow the trend of the forward region. Asymmetric and non-linear J–V curves in the forward region show that these devices exhibit rectification behavior. [Gupta & Singh (2005)] The conduction mechanism in non-linear J–V characteristics could be explained based on thermionic emission. To realize the charge transport in a different region, we have

explored the double log. J–V characteristics in the forward bias condition as demonstrated in Figure 5.15

The graph illustrates three regions and can be categorized as I, II, and III in the double log. J–V plot. These plots can be attributed to ohmic (I region), trap limited space charge limited conduction (TLSCLC) (II region), and trap-free space charge limited conduction (TFSCLC) region (III region), respectively.

We have determined the ideality factor 'η' reverse saturation current density 'J_0' and the barrier potential height 'Φ_B' by using above equations which were extracted from Cheung's idea and listed in table 5.1

Following this model, the intrinsic carrier mobility has been estimated from a higher voltage region of the J vs. V^2 plot (Figure 5.16) by the Mott-Gurney equation

$$J = \frac{9}{8}\mu\epsilon_0\epsilon_r\frac{V^2}{d^3}$$

Where J, ε_0, ε_r, and μ have their usual meaning viz. current density, free space permittivity, relative dielectric constant, and the mobility of the synthesized complex, respectively. The thickness (d) of device was found to be 2 μm via AFM. The relative dielectric constant for the semiconducting gel is 2.62. Using these data, we have calculated the mobility in TFSCLC region and listed in Table 5.1

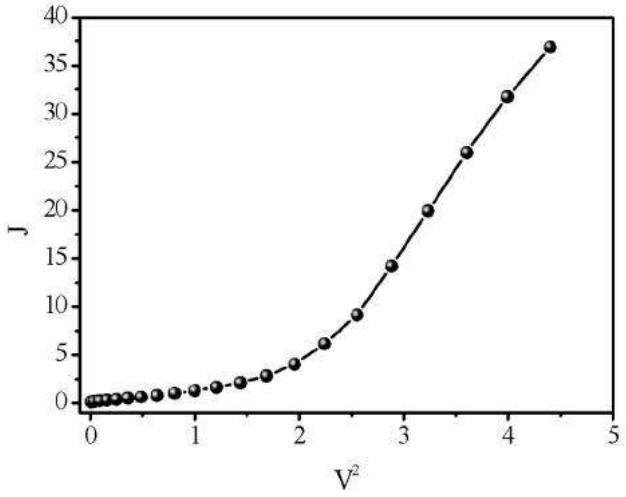

Figure 5.15 J-V^2 characteristics of ITO/SG/Au device.

5.4.12 Investigation of photo-response

Finally, in order to examine the photovoltaic property of complex materials, the sandwiched structure of ITO/semiconducting gel/Al Schottky devices was employed under the illumination of the green wavelength of light. [Buxton & Clarke (2006)] It is noteworthy here that all devices were illuminated from ITO side and photo-response was recorded in the range ±2 V and illumination of the device from the backside demonstrates the enhancements in the current. Semiconducting gel/Au metal junction has been studied, as shown schematically in Figure 5.16. The significant enhancement in current observed in reverse bias condition upon illumination [Singh *et al.* (2014)]. However, in forward bias condition, it remains nearly same as compare to dark current as demonstrated in figure 5.17 the significant increase in the photocurrent of under the reverse bias condition upon illumination were observed due to the formation of the excellent quality junction, which leads to formation of a

robust built-in depletion region for the separation of charge carriers. [Kippelen & Brédas (2009)]

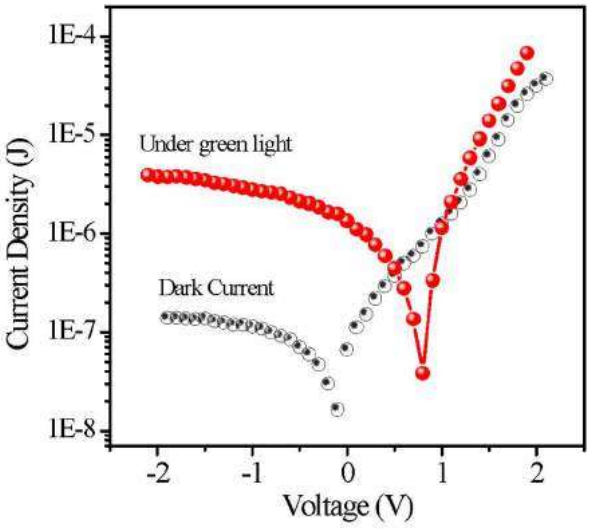

Figure 5.16 J-V characteristics of ITO/SG/Au under the dark condition and illumination of green light

5.5 Conclusion

Simple mixing based strategy for the formation of metallogel by Schiff base gelator has been achieved by using cobalt acetate dihydrate and deprotonated (LiOH) Adipoyl derived hydrazone based gelator at room temperature under atmospheric pressure. Mechanical properties for the coordination polymeric Co(II)-metallogel are scrutinized by rheology, and nanofibrous morphology were observed by using TEM techniques. Electrical and photoelectrical properties were examined and found positive, which indicated its semiconductive nature. Coordination polymeric nature was seen using the ESI-MS technique along with spectroscopic studies by UV-Vis. Overall in this article, we examined a nearly

untouched illustration of coordination polymeric gel in technologically challenging electronic device applications along with photoelectric properties. The rectification ratio (I_{on}/I_{off}) of our device and found to be 266±15, which is very good for semiconducting gel-based newly fabricated devices. The substantial increase in the photocurrent of under the reverse bias condition upon illumination are observed due to the formation of a good quality junction, which leads to the creation of a robust built-in depletion region for the separation of charge carriers. The measured charge transport parameters of the CoA-SHAL based thin-film device are fascinating, embracing the signature of the first CoA-SHAL based electronic device as a Schottky barrier diode.

5.1 Introduction

Gels comprise molecular designs that are proficient at forming 3D spatial arrangement via various chemical interactions; some of the traditional to be mentioned gels are organogel, hydrogel, and supramolecular gels [Hirst *et al.* (2008), Lan *et al.* (2015), Sugiyasu *et al.* (2004), Miyata *et al.* (1999), Sangeetha & Maitra (2005)]. Wherein, metallogel gaining a swift as an imperative bough of supramolecular gels [Tam *et al.* (2013)]. With the distinct choice of gelator moiety and transition metals, they were formed when a metal complex self-assembles by capitalizing non-covalent interactions to fabricate vastly cross-linked, entwined, the three-dimensional framework to immobilize a large number of solvent molecules [Svobodová *et al.* (2012), Venkataraman *et al.* (2011)]. It is valuable to cite that in a sprint towards gel formation, self-assembly progression in a one-dimensional manner engenders fibrous morphology. Introducing functional groups like urea, amide, and aromatic rings, which are capable of shaping various weak interactions like hydrogen bonding or π–π stacking in amid combination of suitable gelator and transition metals, are very much influential in immobilizing solvent.

Meanwhile, multiple coordinating sites in ligands uphold the obligatory cross-linked network in gel, but superficially exo-diatopic ligand with a "one dimensional'' approach in the majority was put into operation for metallogels synthesis [Liu *et al.* (2016)]. This observation goes in opposition to the fundamental principle of gel formation but favors solid polymeric coordination polymers or MOFs, notwithstanding widespread efforts of the hard-working scientific commune.[Kurth & Higuchi (2006)] It is still nearly impossible to predict the design of a gelator molecule like a fixed thumb rule. The Modular character of

metallogel, owe them an assortment of responsive assets with critical potential applications, including chemodosimetry, cosmetics, light-harvesting material, catalytic screening, biochemical and biomedical as well as photonic applications [Whittell *et al.* (2011), Borré *et al.* (2016), Yan *et al.* (2012), Pandey *et al.* (2017), Tam & Yam (2013), Miao *et al.* (2013), Tu *et al.* (2011), Martínez-Calvo *et al.* (2015),Chen *et al.* (2015), Sutar & Maji (2016), Howlader & Mukherjee (2016), Gasnier *et al.* (2009), Steed (2010)].

In contrast, to remarkable physic-ochemical properties such as magnetic, spectroscopic, and catalytic properties, this human-made molecular congregation of soft materials in the utmost of the cases, cannot be directly applied to other useful applications, particularly in electronic devices [Amacher *et al.* (2015), Mitsumoto *et al.* (2017)]. Therefore, the dominance of inorganic materials has stayed ascertained for the fabrication of durable electronic devices [Sun *et al.* (2017)]. Nonetheless, in a pursuit to augment performance and miniaturization of the device and to reinstate the usual inorganic semiconductors, technological advancement attains newer heights towards organic/plastic electronics with functional materials of natural origin. A very few reports were taken up on gel-based π-systems with high conducting properties in oligo(thienylenevinylene) based-organogelator by Ajayaghosh and his co-workers [Praveen *et al.* (2016), Siddhanta & Gangopadhyay (2005)]. In a very similar manner, nanorods and nanotapes with soaring charge carrier mobility were observed as well, while Zang and co-workers performed the groundbreaking synthesis of perylenebisimide-based photo conducting nanofibril, nanoribbons and nanobelts [Che *et al.* (2007)]. An apparent severity in sophisticated molecular designing and synthesis, with tedious optimization to avoid charge carrier

recombination of the intermolecular assembly, makes them very much unreasonable towards large-scale application. [Beaujuge & Fréchet (2011)]

Performances of semiconducting materials are crucially dependent on movement efficiency of charge carriers poignant within the assembled π-conjugated system and hence developing effortless schemes towards the fabrication of photo-conducting materials [Mitsui *et al.* (2014)]. In this article, we reveal the preparation of a Schiff base derived polymeric coordination gel, with high efficiency *en-route* to functioning as semiconducting devices. Reports on conducting gels are escalating but homologically constrained to systems like tetrathiafulvalene (TTF), thienylenevinyle, etc. Here we have been able to apply these materials successfully in metal-semiconductor junction thin-film devices to study the electronic device applicability and charge transport properties of the synthesized material. The current-voltage characteristics of our fabricated devices depict a non-linear rectifying nature, similar to a Schottky barrier diode with a sound rectification ratio [Bhattacharya *et al.* (2014), Dhibar *et al.* (2018)]. Hence we have analyzed the device performance of our fabricated Co metallogel based Schottky diode.

5.2 Instrumentation

Electronic absorption spectra was obtained on a Thermo scientific EVOLUTION 201 spectrophotometer. ^{1}H NMR spectra was collected on a Bruker AVANCE III HD 500 spectrometer. Electrospray ionization mass (ESI-MS) spectra were recorded on a Waters (Micromass MS Technologies) QTof Premier. Thermal Gravimetric analysis data was acquired on a NETZSCH STA 449 F3 at a heating rate of 5 °C min^{-1} under a nitrogen atmosphere. TEM images. Powder XRD data were collected on Rigaku MiniFlex 600

Detector D-tex ultra between angle 2θ = 5-80°. Solution electrical conductivity was measured on a Eutech Instruments CON 5/TDS 5 Conductivity Meter. The instrument was calibrated with standard solution. All rheological measurements of metallogel were performed on Anton Paar MCR 702 Twin Drive Rheometer. A Kiethley Source meter model number 2612 was used to perform the current-voltage (I–V) characteristics of our manufactured coordination polymeric gel material based thin film devices.

5.3 Experimental Section

5.3.1 Method

5.3.1.1 Synthesis of Gelator SHAL

To a methanolic suspension of adipoyl hydrazone (1.00g, 6.8 mmol), 2 mL water is added to obtain a clear solution. 2-hydroxybenzaldehyde (1.67 g, 13.6 mmol) was added to this solution and refluxed for 1 hour. The precipitate obtained after cooling to room temperature was filtered, thoroughly washed with Chloroform, methanol, and Hexane to afford a white solid (AL), Yield 1.74 g (81 %). Due to deprived solubility of the neutral form, UV-vis measurements is performed by dissolving the solid in DMF in the presence of 1 Equivalent of LiOH [Pandey *et al.* (2019)].

5.3.2 Synthetic Scheme of Gelator

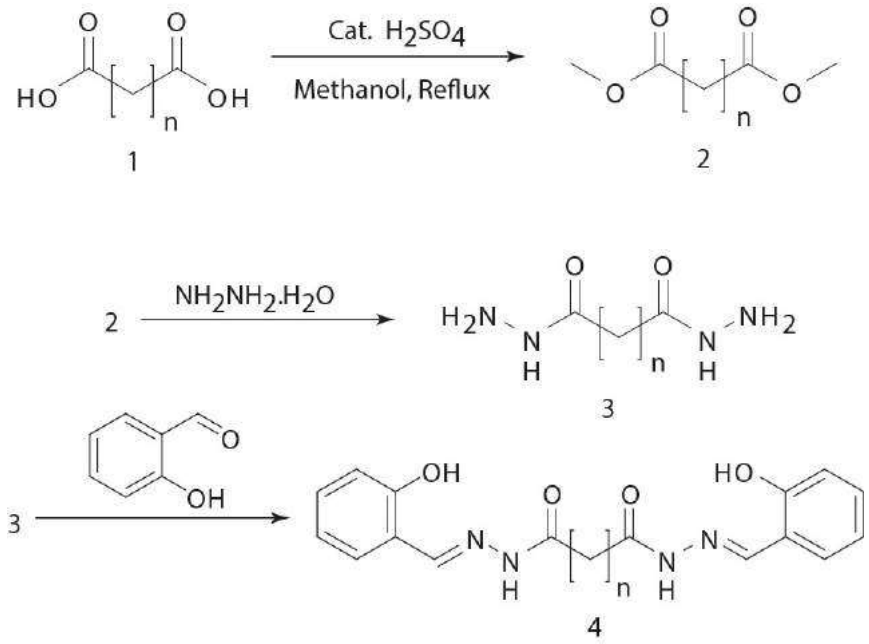

Scheme 5.1 Synthetic Strategy adopted for the synthesis of gelator SHAL

5.3.3 Preparation of metallogel

An unambiguous, transparent solution was prepared upon mixing SHAL (10 mg, 0.026 mmol) in 0.5 mL DMF and 4 equivalents LiOH (4.37 mg, 0.10 mmol in 0.25 mL DMF) followed by brief sonication. For gelation, a solution of $Co(OAc)_2 \cdot 4H_2O$ (6.94 mg, 0.026 mmol in 0.25 mL) was added instantly to previously prepared mixture of SHAL deprotonated with LiOH, a translucent & non-fluorescent brown color gel (1% w/w) was formed within a minute at room temperature under atmospheric pressure (Scheme 5.1). The CoA-SHAL coordination polymeric gel was stable for an extended period of even two weeks.

5.4 Results and Discussion

5.4.1 Characterization

The synthesized metallogel is characterized by various instrumental techniques such as ^{1}H NMR and IR spectrometry **(**Figure 5.2**)**.

5.4.2 ^{1}H-NMR and IR spectrum of gelator

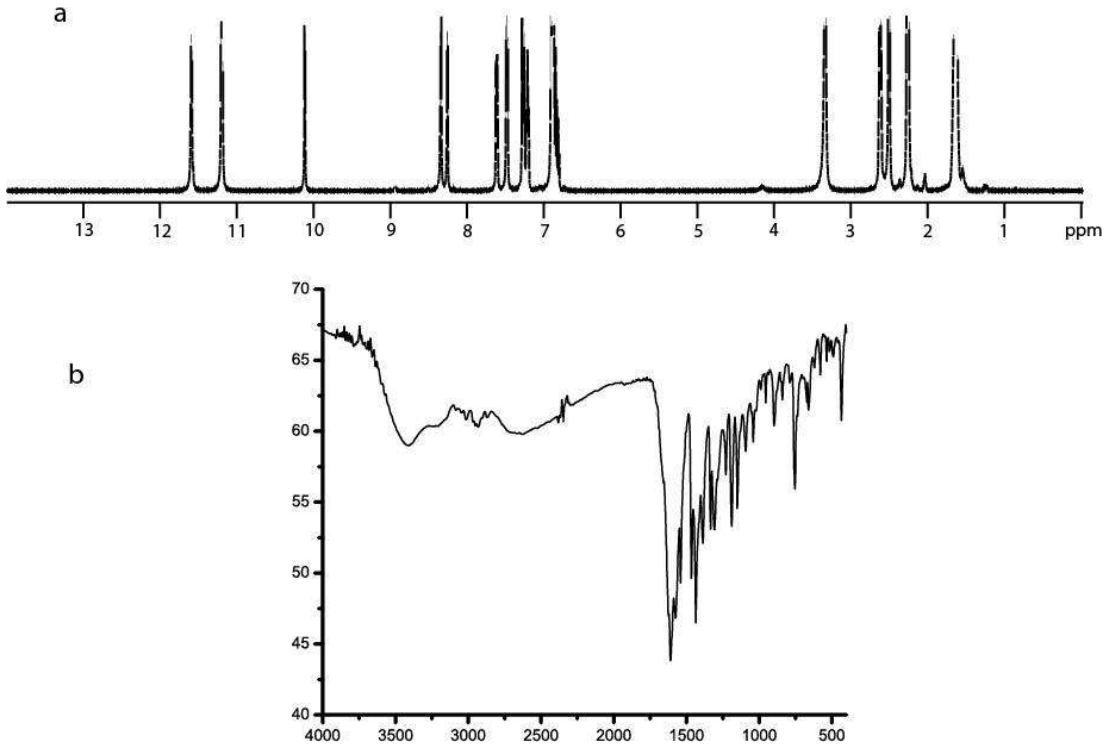

Figure 5.1 ^{1}H NMR and FTIR spectra of gelator SHAL

5.4.3 Comparative IR of gelator and metallogel

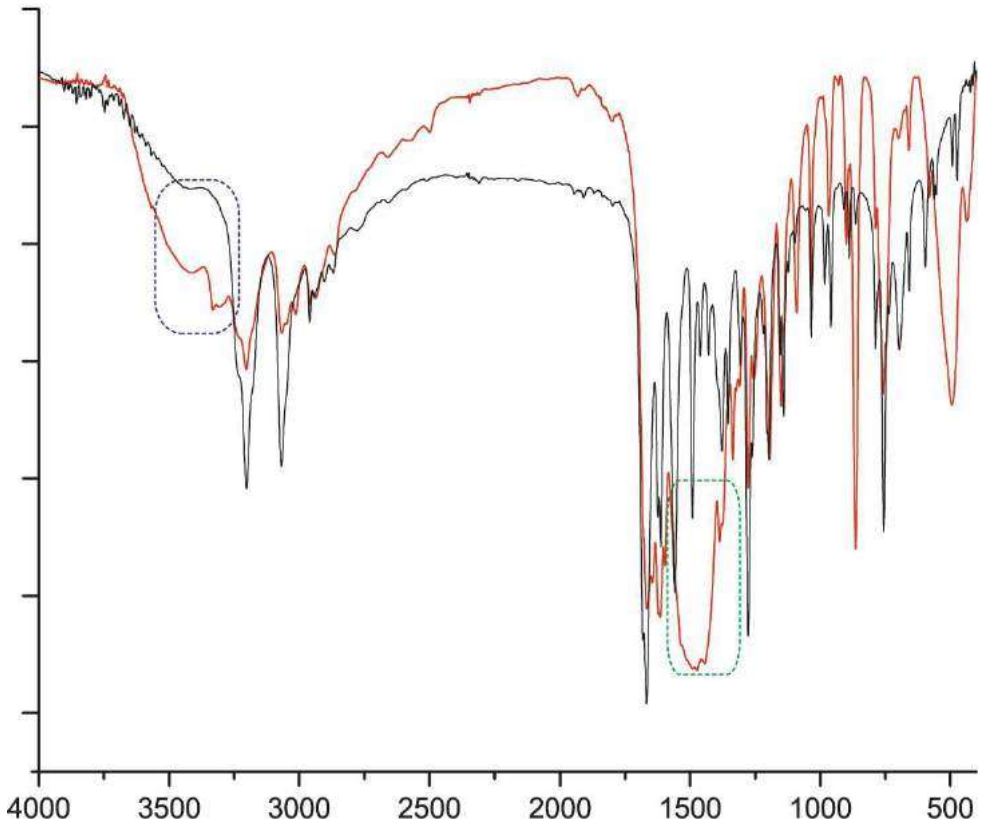

Figure 5.2 Comparative IR spectra of gelator (black) and xerogel (red) showing coordination of Co^{2+} through O, N, O binding core

FTIR spectral analysis (Figure 5.2) of Schiff base gelator (SHAL) shows characteristic bands of υ(–OH), υ(–NH) at 3407 cm^{-1} and 3206 cm^{-1}, respectively, while active band at 1669 cm^{-1} is corroborated to υ(-C=O) group, in addition to peaks as mentioned earlier υ(–C=N) is observed at 1553 cm^{-1} which suggest the enolic form of ligand. A comparative study of FTIR spectra of gelator and xerogel SHAL indicates the disappearance of –OH band, broadening of aforementioned N-H band, and shifting of υ(–C=O) to 1606 cm^{-1} ($\Delta\upsilon$ = 53 cm^{-1}) which may be attributed to the coordination of Co^{2+} through O, N, O binding

core. Alkali base (4 equiv.) is required for deprotonation signifies the tetra basic hexadentate nature of ligand as it is a necessary condition for coordination of a metal ion through deprotonation of both phenolic and -NH labile protons adjacent to azo-methine group [Pandey *et al.* (2019)].

5.4.4 Mechanical Properties of metallogel

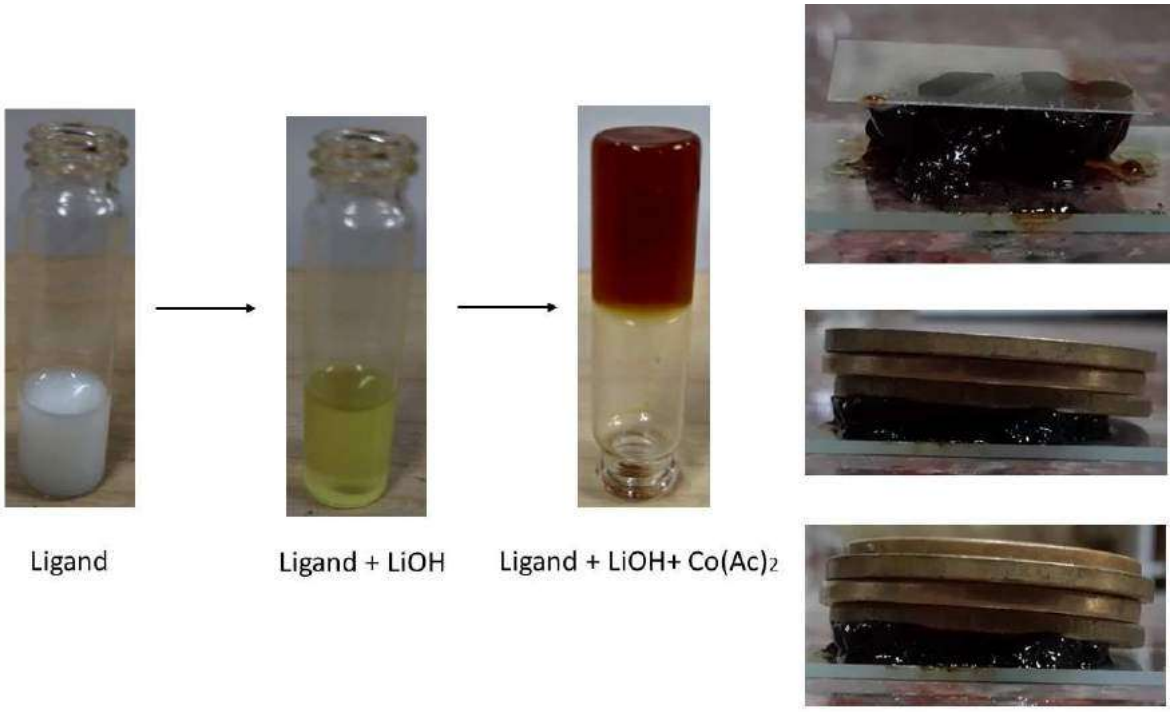

Figure 5.3 mechanical and load bearing properties of Cobalt containing metallogel

Excellent load-bearing and mechano-responsive behavior is observed with metallogel. Gel formation was extremely fast without the help of any external stimuli.(Figure 5.3)

5.4.5 Morphology of Metallogel

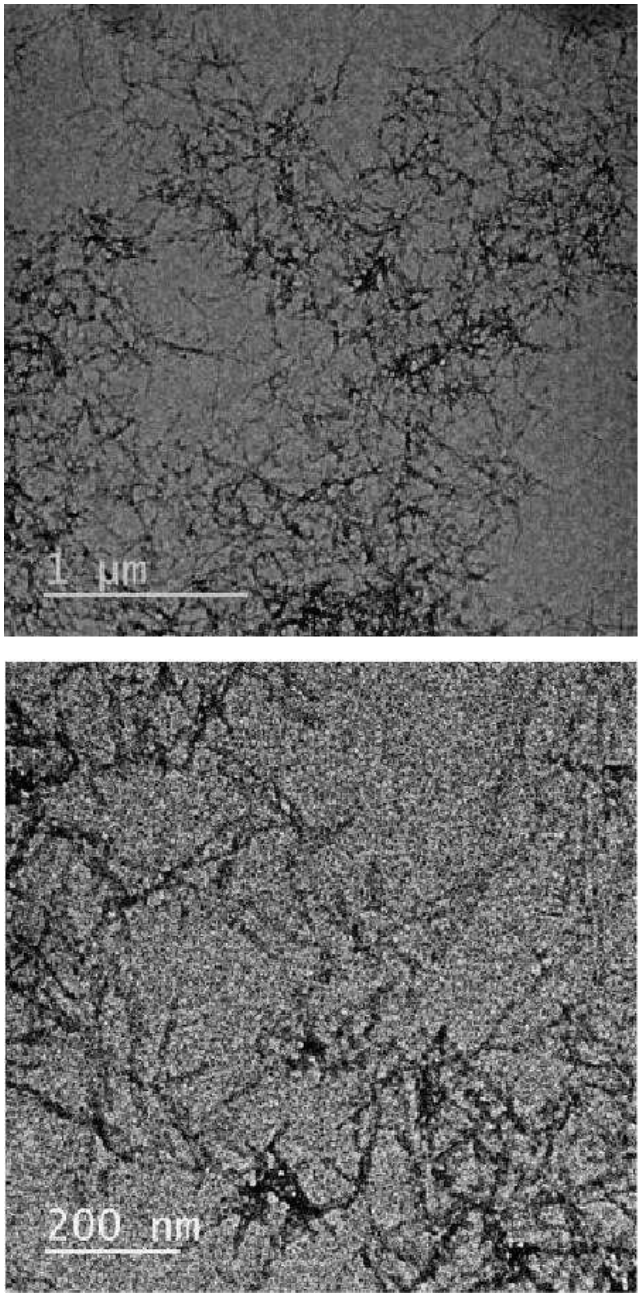

Figure 5.4 TEM pictures of diluted metallogel (SHAL/LiOH/$Co(OAc)_2$; ~10^{-3} M) under three different magnifications

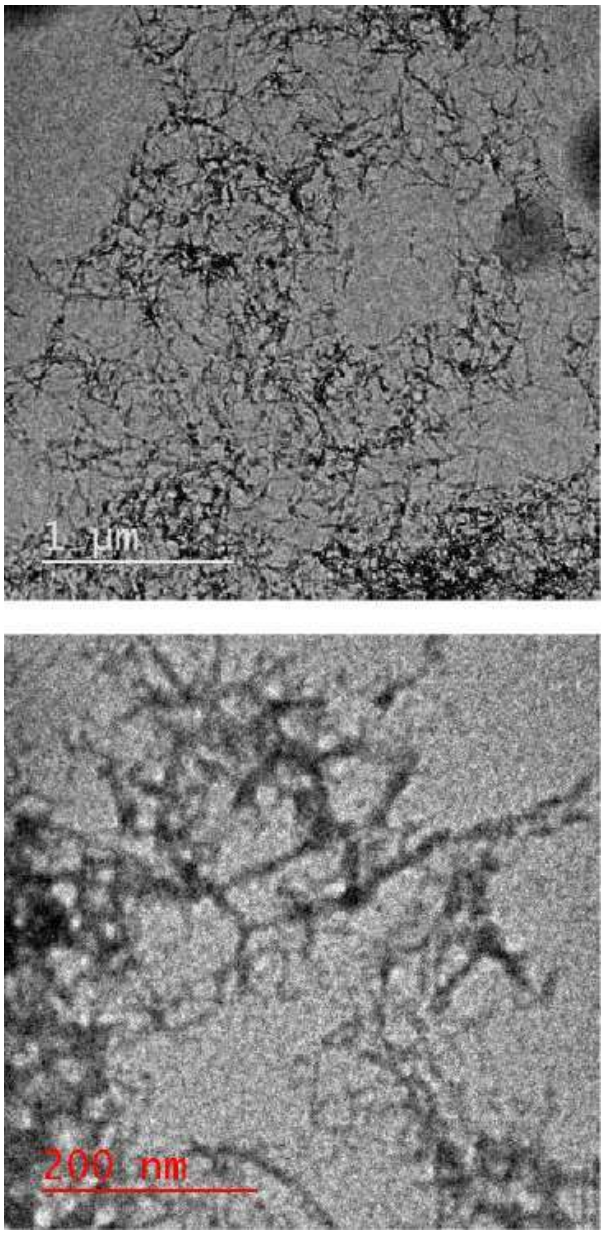

Figure 5.5 TEM pictures of diluted metallogel (SHAL/LiOH/$Co(OAc)_2$; ~10^{-3} M) under three different magnifications

Unambiguous morphological insights of obtained metallogel is examined under Scanning Electron Microscopy (SEM) and transmission electron microscopy (TEM).

Interesting observations are obtained upon its comparison to our previously reported work. Morphology revealed by SHAL derived gel was also in line with the above statement, where TEM (Figure 5.4) revealed the bunch of extended and interconnected fibers with close-knitted appearance. TEM (Figure 5.5) study on diluted metallogel revealed the three-dimensional (3-D) network of nanofibers of about ~25 nm in average diameter with an intermingled appearance

5.4.6 UV-vis Spectroscopy

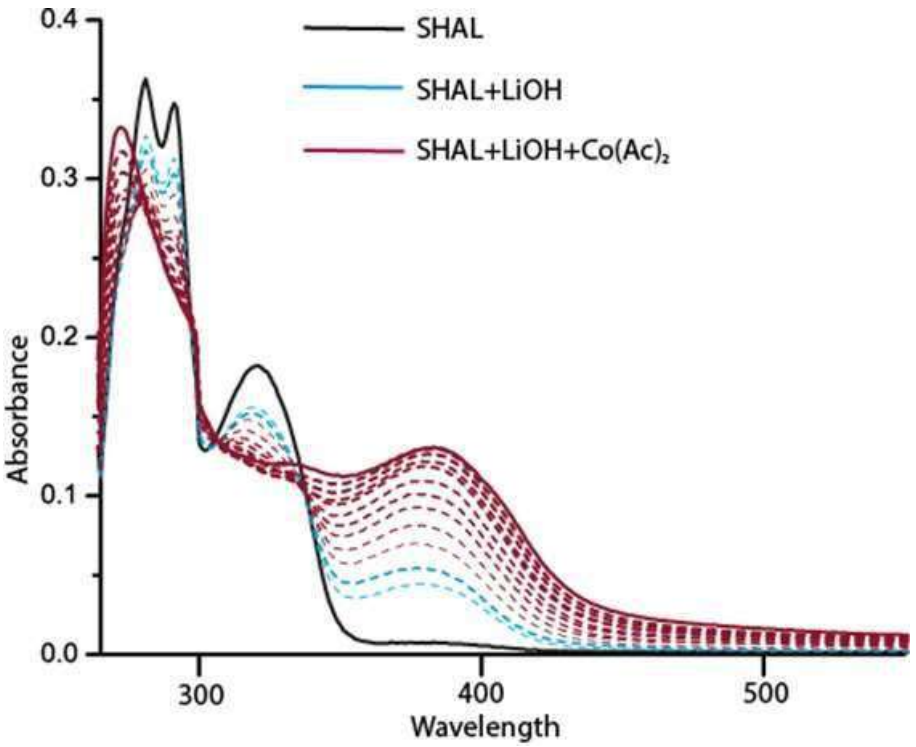

Figure 5.6 UV-vis titrations in DMF (a) ligand SHAL, (black line; λ_{max} 320 nm; 1x10^{-5} M), deprotonation with LiOH (4 equiv., blue line) and upon aliquot addition of Co(OAc)$_2$ (red line) band corresponding to ligand diminishes ratio-metrically with appearance of new peak at 388 nm along with fine isosbestic point

To prove the complexation between SHAL and Co(II) as well as gelation behavior, we executed detailed electronic absorption studies. Exposition of two vividly coupled bands

by SHAL ($1x10^{-5}$ M, DMF, 298 K) at λ_{max}=280 nm and 291 nm are accredited to intraligand π-π* transition while a less intense band at 320 nm endorsed n-π* transition [Pandey *et al.* (2017)].

Alternatively, splitting of the peak at 280 and 291 nm elucidate dissimilar planarity of both hydrazones, i.e., both free hydrazones exist in anti-cis configuration. Inconsequential variation in spectra are observed upon deprotonation of SHAL ($1x10^{-5}$ M, DMF) with 4 eq. LiOH, i.e., a light yellow colored solution of SHAL displayed a hump at about 394 nm with a concomitant decrease of the 320 nm band along with the ratiometric increase of hump. It indicates deprotonation of phenolic –OH as well as chelation of Li^+ with SHAL in N,O fashion. While upon aliquot addition of $Co(Ac)_2.4H_2O$ ($1x10^{-3}$ M, DMF) to this solution, the disappearance of band at 320 nm is observed with ratiometric emergence of a new peak at 388 nm ($\Delta\lambda$ = 68 nm) (Figure 5.6). Two nice isosbestic points at 305 and 344 nm indicate the presence of equilibrium between two species during their transformation to the coordination complex. The endpoint of UV titrations is found to be 1.0-1.2 equivalent indicated the formation of a coordination complex, between Co(II) with SHAL at 1:1 ratio. Stoichiometry model for Co^{2+} complexation with gelator SHAL demonstrated through Job's plot was found in good agreement to above spectroscopic result where the gelling combination was found close to 1:1 metal to ligand ratio (Figure 5.7**)**.

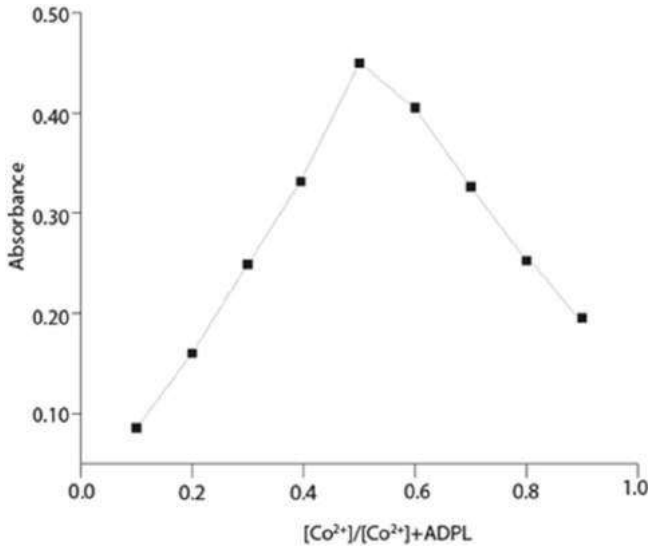

Figure 5.7 Job's plot diagram of [Co^{II}]/[Co^{II}]+[SHAL]

5.4.7 Emission Spectroscopy

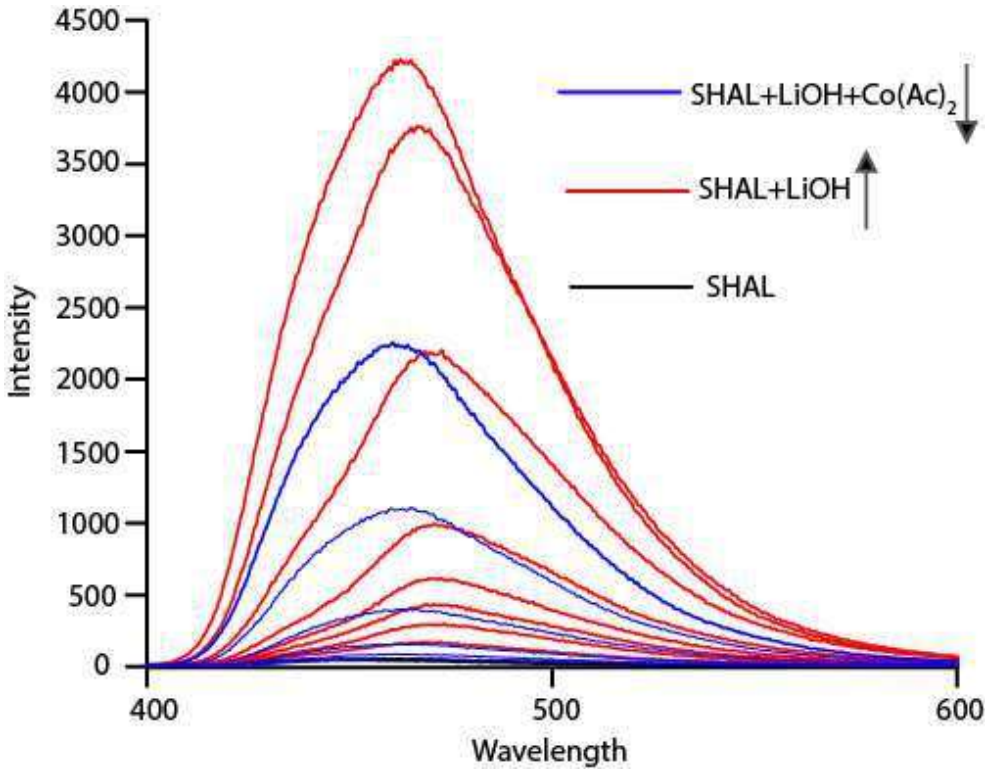

Figure 5.8 Fluorescence spectra in DMF (Red line = deprotonated ligand, Blue line = Metal addition (λ_{ex} = 320 nm)

In the course to reconnoiter the aggregation behavior as well as mechanistic acuity towards gelation, fluorescence experiment were performed over non-fluorescent metallogel (Figure 5.8**)**. The non-fluorescent nature of SHAL (λ_{ex}=320 nm, λ_{em}=477 nm, stokes shift= 10300 cm^{-1}; $1x10^{-3}$ M, DMF, black line) transformed subsequently to bluish-green fluorescent solution upon ratio-metric deprotonation with LiOH (10^{-1} M, DMF, red line) and showed peak at 471 nm (stokes shift= 10150 cm^{-1}; red line) with noticeable enhancement in fluorescence intensity which can be credited to chelation of Li^{+} to AL^{2-} and can be ascribed to well-known phenomenon of chelation enhanced fluorescence (CHEF) as in our previous report where large enhancement of fluorescence is observed through CHEF upon LiOH addition to the ligand. Further, we observed quenching upon addition of the requisite amount of Co^{2+} (10^{-1} M, DMF, blue line) required for metallogel formation (λ_{em}=468 nm, stokes shift= 9900 cm^{-1}; blue line) indicates the presence of ACQ phenomenon in gelation process [Pandey *et al.* (2017)].

5.4.8 ESI Mass analysis of metallogel

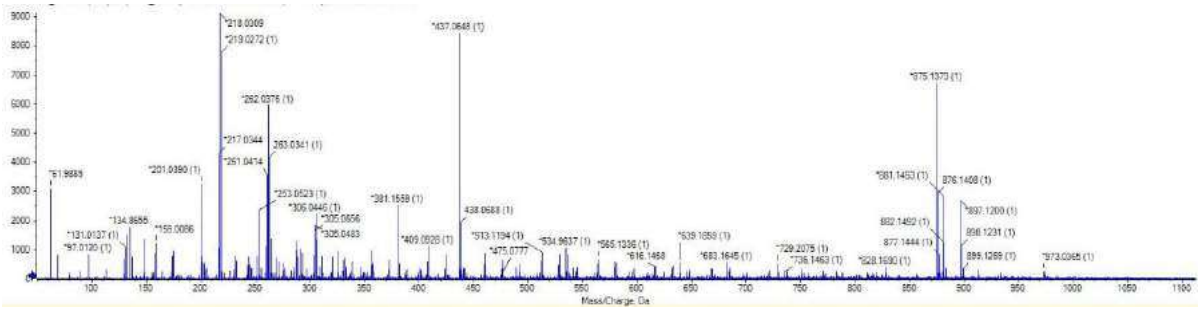

Figure 5.9 ESI-MS spectra of $[(C_{20}H_{21}N_4O_4)Co_2Li_5)]^-$ at 534.96 represents the experimental isotopic abundance pattern 1:1 polymeric coordination SHAL vs Co^{2+} repetitively (1 ligand + 2 metal ion in one asymmetric unit)

To ensure the formation of coordination complex indicated by UV-vis and Job's plot, we performed detailed ESIMS spectral analysis over diluted metallogel. ESI-MS spectra of

$[(C_{20}H_{21}N_4O_4)Co_2Li_5)]^-$ at 534.96 represents the experimental isotopic abundance pattern 1:1 coordination polymeric SHAL vs. Co^{2+} in a repetitive manner. (Figure 5.9)

5.4.9 Rheology

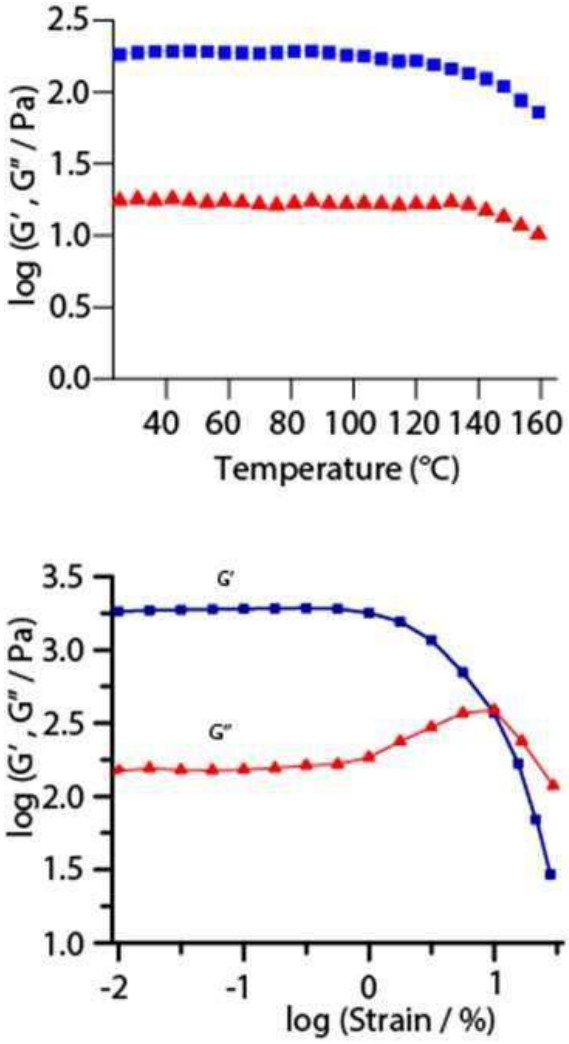

Figure 5.10 (upper) Dynamic temperature ramp G' and G'' for SHAL-Co gel at heating rate of 1°C min^{-1}, strain of 0.5% and frequency of 1 rad s^{-1}, (lower) Dynamic oscillation strain sweep of G' and G'' for gel at frequency of 1 rad s^{-1} and 25 ° C

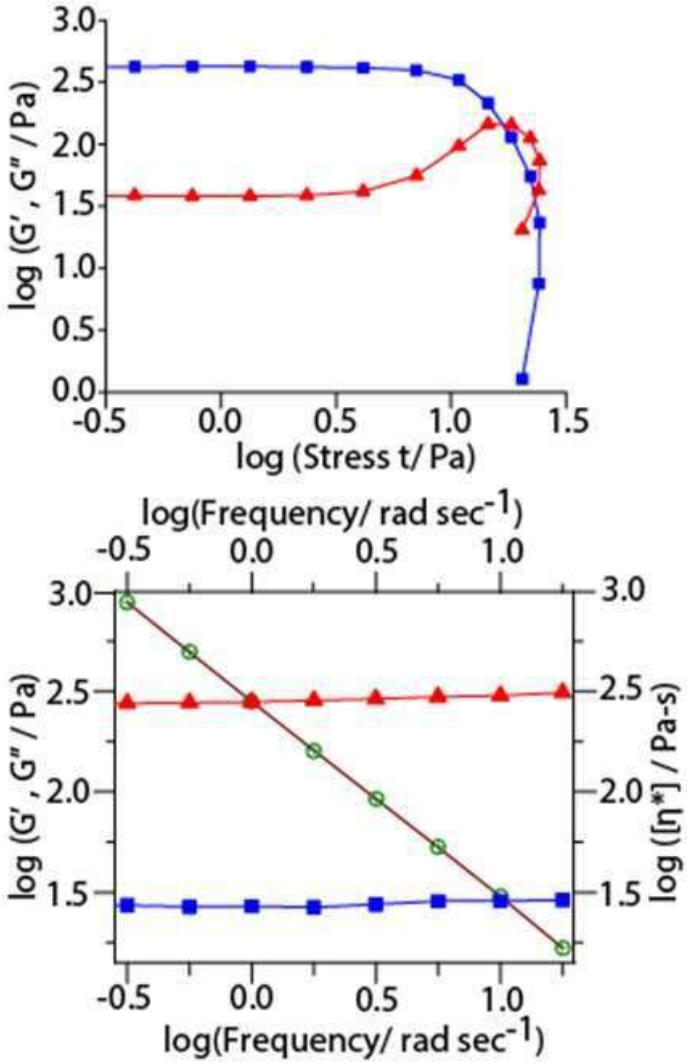

Figure 5.11 (upper) Dynamic shear stress of G' and G'' for gel, (lower) Dynamic frequency sweep measurement of G' and G'' for SHAL-Co gel at strain of 0.5%. Secondary axis: complex viscosity measurements

Rheological experiments are conducted over freshly prepared (1.0% w/v) fixed concentration metallogel. Implementation of frequency sweep measurements between 0.1 and 100 rad s^{-1} at 25°C within the linear viscoelastic region indicated that G' and G'' values were linear and increase slightly within the applied frequency (f) range (-1.0-2.0 rad s^{-1}) principally supporting its elastic nature. Furthermore, G' is dominating G'' and they do not

cross each other, suggesting any phase separation or transition, which is anticipated for a stable and rigid gel phase material. Further evidence of elasticity was visualized by the fact that G' and G'' are very less sensitive to angular frequency (ω). Variation tendency of both storage modulus (G') and loss modulus (G'') with increasing temperature was recorded from temperature range 25-160°C. As shown in (Figure 5.11), both values remain unaffected up to 120° C and above which both G' and G'' decreases with an inclination in temperature, indicating liquefaction. Storage Modulus (G') and loss modulus (G") are obtained at 25°C and 1 rad s^{-1} as a function of shear stress and strain (Figure 5.10 and 5.11). Metallogels when subjected to oscillatory shear, value of G' was found be higher than G'' by order of ~1 magnitude of shear stress. It is in accordance with the exact gel phase where no variation among G' and G'' was observed with appreciable long range of increasing applied stress. At yield stress of ~1.3 Pa G' and G'' intersect each other establishing a mechanical breakup of gel beyond which the deviation from linearity results in a gel-sol phase transition. On the other hand, both in-phase storage modulus (G') and out-of-phase loss modulus (G'') remain constant up to 0.9% (G'>G''), beyond which deformation of network occurred.

5.4.10. Optical characterization

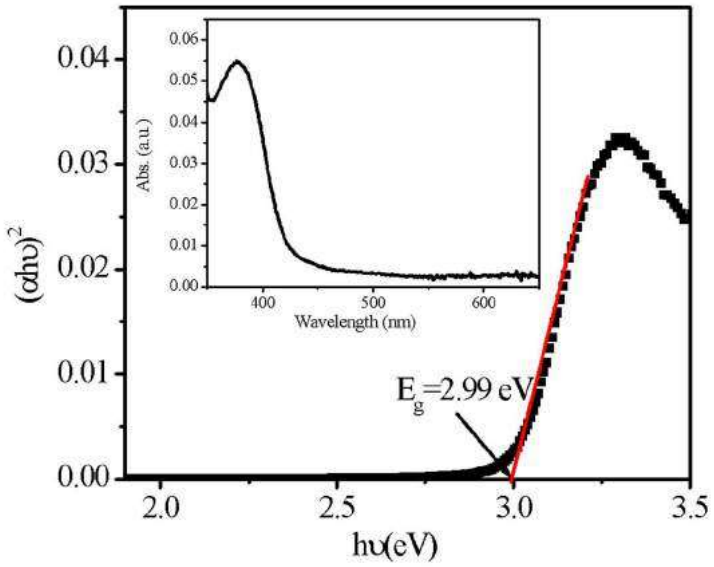

Figure 5.12 Electronic absorption spectra (inset) and Tauc's plots for semiconducting gel film

To examine the spectral property and estimation of the bandgap, the electronic absorption spectrum of thin film was recorded in the range 250–600 nm using UV-vis spectrophotometer [Radecka *et al.* (2008)] as shown in Figure 5.12, The direct optical band gap of the film can be calculated by applying Tauc's equation,

$$(\alpha h\nu)^2 = A\,(h\nu - E_g)$$

where α, E_g, h and ν denotes absorption coefficient, the band gap of materials, Planck's constant, and frequency of light, respectively. We have extrapolated the linear region of the plot $(\alpha h\nu)^2$ vs. hν, as demonstrated in Figure 5.13. The value of E_g of the film of the material has been calculated as 2.99 eV.

5.4.11. Electrical Characterization

Our previous investigation in this report and published literature suggests that our synthesized complex is an n-type semiconductor material in nature. Therefore, we have fabricated the sandwiched structure of the metal-semiconductor junction using suitable electrode materials and studied its electrical properties by analyzing the charge transport behavior [Kahn *et al.* (2003)]. It is worth here to mention that the junction properties of semiconducting materials were determined by the interfacial properties of two electrodes used for device fabrications and the difference of their respective work functions [Tada et al. (2011)]. Therefore, for fabrications of a diode having rectifying behavior, one should select an electrodes materials in such a way that one electrode work as ohmic contact and other electrode creates non-ohmic Schottky contact with semiconducting layer. As per the theory of the Schottky barrier, the work function of the metal electrode should be higher as compared to the n-type semiconductor for the creation of a rectifying barrier at the interface [Tongay *et al.* (2012)]. As stated in published articles, the work function of indium tin oxide (ITO) is comparable with our materials and form an ohmic contact. However, gold (Au) creates rectifying contact due to a higher work function. Therefore, we select these materials for the formation of rectifying Schottky diode [Lu *et al.* (2006)].

The current density-voltage (J-V) measurements of our synthesized complex based multiple devices are recorded at a corresponding applied bias voltage sequentially within the limit ±2 V and analyze for various electrical parameters [Aswal *et al.* (2006)]. The J–V characteristics of the synthesized complex-based devices have been investigated at room temperature under the dark condition and are demonstrated in Figure 5.13 the recorded J–V characteristics of the Au/semiconducting gel interface show an asymmetrical nonlinear

nature curve, which is the validation of a rectifying Schottky barrier diode (SBD). We have calculated the rectification ratio (I_{on}/I_{off}) of our device and found to be 266±15, which is very good for the semiconducting gel-based newly fabricated device [Capozzi *et al.* (2015)].

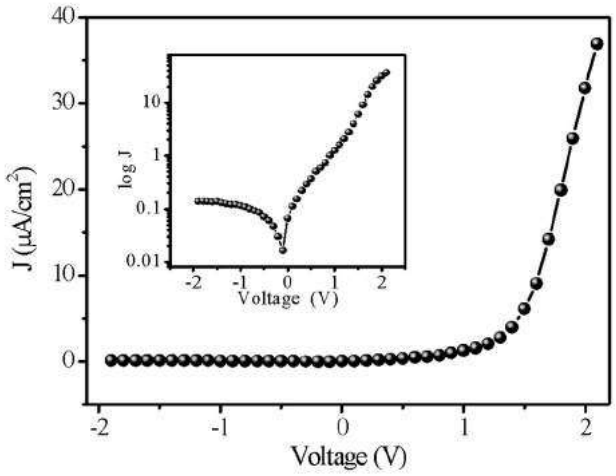

Figure 5.13 J–V characteristics curve for ITO/complex/Au structured thin film devices at room temperature

The obtained rectifying J-V characteristics of semiconducting gel at room temperature were further analyzed by assuming the standard thermionic emission theory and Cheung's method and extracted critical electrical parameters of the device. [Dragoman & Dragoman (2004)] To analyze J-V curves quantitatively, we have first employed the following standard equations:

$$J = J_0 \exp(\frac{qV}{\eta kT})(1 - \exp(\frac{-qV}{\eta kT}))$$

At room temperature, $J_0 << 1$. Therefore

$\eta = \frac{qdV}{kTdln(J/J_0)}$ and

$J_0 = A^*T^2\exp(\frac{-q\Phi_B}{kT})$ or $\Phi_B = \frac{kT}{q}\ln(\frac{A^*T^2}{J_0})$

where J_0, k, T, V, A, η, and A* demonstrate the reverse saturation current, electronic charge, Boltzmann constant, temperature in Kelvin, forward bias voltage, ideality factor, and effective Richardson constant, respectively. The effective Richardson constant may be considered as 32 A K^2 cm^{-2} for the semiconducting gel-based devices.

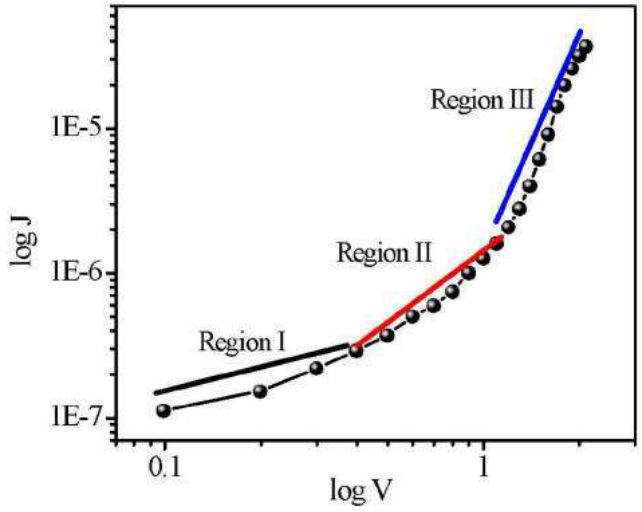

Figure 5.14 Double log plot of J-V characteristics.

Table 5.1 Electronics parameter of device

Device	η	J_0 A/cm^2	Φ_B(eV)	M (cm^2/V.s)	I_{on}/I_{off}
ITO/SG/Au	3.1	$1.64x10^{-8}$	0.89	$4.36x10^{-4}$	266±15

In the forward region, current increases exponentially while in reverse region current do not follow the trend of the forward region. Asymmetric and non-linear J–V curves in the forward region show that these devices exhibit rectification behavior. [Gupta & Singh (2005)] The conduction mechanism in non-linear J–V characteristics could be explained based on thermionic emission. To realize the charge transport in a different region, we have

explored the double log. J–V characteristics in the forward bias condition as demonstrated in Figure 5.14

The graph illustrates three regions and can be categorized as I, II, and III in the double log. J–V plot. These plots can be attributed to ohmic (I region), trap limited space charge limited conduction (TLSCLC) (II region), and trap-free space charge limited conduction (TFSCLC) region (III region), respectively.

We have determined the ideality factor 'η' reverse saturation current density 'J_0' and the barrier potential height 'Φ_B' by using above equations which were extracted from Cheung's idea and listed in table 5.1

Following this model, the intrinsic carrier mobility has been estimated from a higher voltage region of the J vs. V^2 plot (Figure 5.15) by the Mott-Gurney equation

$$J = \frac{9}{8}\mu\epsilon_0\epsilon_r\frac{V^2}{d^3}$$

Where J, ε_0, ε_r, and μ have their usual meaning viz. current density, free space permittivity, relative dielectric constant, and the mobility of the synthesized complex, respectively. The thickness (d) of device was found to be 2 μm via AFM. The relative dielectric constant for the semiconducting gel is 2.62. Using these data, we have calculated the mobility in TFSCLC region and listed in Table 5.1

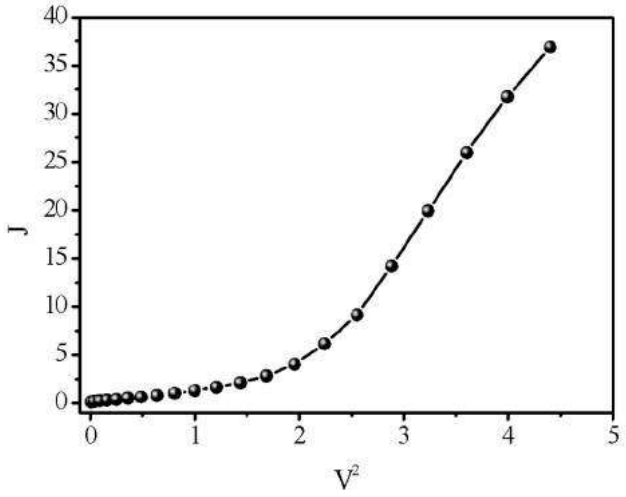

Figure 5.15 J-V^2 characteristics of ITO/SG/Au device.

5.4.12 Investigation of photo-response

Finally, in order to examine the photovoltaic property of complex materials, the sandwiched structure of ITO/semiconducting gel/Al Schottky devices was employed under the illumination of the green wavelength of light. [Buxton & Clarke (2006)] It is noteworthy here that all devices were illuminated from ITO side and photo-response was recorded in the range ±2 V and illumination of the device from the backside demonstrates the enhancements in the current. Semiconducting gel/Au metal junction has been studied, as shown schematically in Figure 5.16. The significant enhancement in current observed in reverse bias condition upon illumination [Singh *et al.* (2014)]. However, in forward bias condition, it remains nearly same as compare to dark current as demonstrated in figure 5.17 the significant increase in the photocurrent of under the reverse bias condition upon illumination were observed due to the formation of the excellent quality junction, which leads to formation of a

robust built-in depletion region for the separation of charge carriers. [Kippelen & Brédas (2009)]

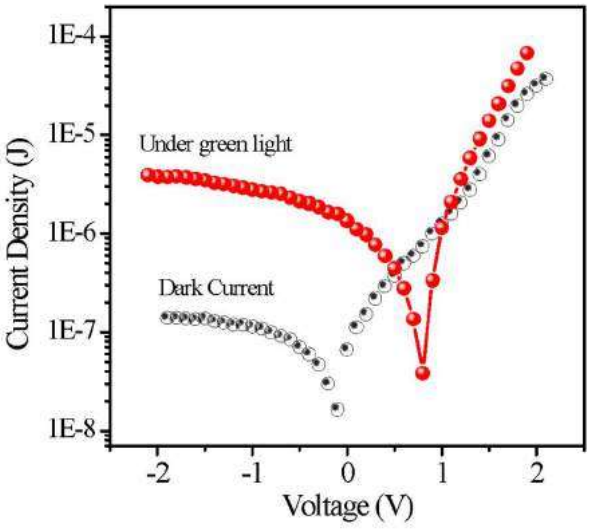

Figure 5.16 J-V characteristics of ITO/SG/Au under the dark condition and illumination of green light

5.5 Conclusion

Simple mixing based strategy for the formation of metallogel by Schiff base gelator has been achieved by using cobalt acetate dihydrate and deprotonated (LiOH) Adipoyl derived hydrazone based gelator at room temperature under atmospheric pressure. Mechanical properties for the coordination polymeric Co(II)-metallogel are scrutinized by rheology, and nanofibrous morphology were observed by using TEM techniques. Electrical and photoelectrical properties were examined and found positive, which indicated its semiconductive nature. Coordination polymeric nature was seen using the ESI-MS technique along with spectroscopic studies by UV-Vis. Overall in this article, we examined a nearly

untouched illustration of coordination polymeric gel in technologically challenging electronic device applications along with photoelectric properties. The rectification ratio (I_{on}/I_{off}) of our device and found to be 266±15, which is very good for semiconducting gel-based newly fabricated devices. The substantial increase in the photocurrent of under the reverse bias condition upon illumination are observed due to the formation of a good quality junction, which leads to the creation of a robust built-in depletion region for the separation of charge carriers. The measured charge transport parameters of the CoA-SHAL based thin-film device are fascinating, embracing the signature of the first CoA-SHAL based electronic device as a Schottky barrier diode.